Development of Electromagnetic Micro-Energy Harvesting Device

by

Pratik Patel

A thesis
presented to the University of Waterloo
in fulfillment of the
thesis requirement for the degree of
Master of Applied Science
in
Mechanical Engineering

Waterloo, Ontario, Canada, 2013

AUTHOR'S DECLARATION

I hereby declare that I am the sole author of this thesis. This is a true copy of the thesis, including any required final revisions, as accepted by my examiners.

I understand that my thesis may be made electronically available to the public.

Abstract

The use of energy harvesting devices has generated much research interests in recent years. There are numerous energy harvesters available in the market that are piezoelectric, electromagnetic, electrostatic or combination of piezoelectric and electromagnetic. Many of the harvesters have shown great potential but are either severely limited in power generation since they are actually never optimized to its potential. One of the goals of this thesis is to develop an electromagnetic micro-energy harvester that is capable of working at low frequencies (5-30 Hz) and is capable of producing electrical power for small devices.

Generally, batteries have been used to power low voltage electronics, however the need for self-sustaining and reliable power source have always been a major issue. This project aims to make a harvester of size AA battery that can be used as a reliable and continuous source of power for bio-medical as well as industrial applications.

Firstly, a linear harvester is developed for applications where there is no set natural frequency. The linear harvester consists of a stator and a mover. The stator includes copper coils, outer iron case and delrin holder for the coils while the mover consists of permanent magnets, iron pole and cylindrical rod. The working principles developed are used to optimize and improve the efficiency of energy harvesting system. The linear harvesting system is tested with the permanent magnet to iron pole ratio $\left(\tau_m/\tau_p\right)$ of 1.25 and permanent magnet to coil ratio $\left(r_p/r_s\right)$ of 0.73. The power density of the linear harvester is determined to be 4.44e-4 W/cm^3. Thereafter, optimization is done in comsol to improve the performance of the energy harvesting system. The optimized magnet to iron ratio is determined to be $\left(\tau_m/\tau_p\right)$ of 3.175 and $\left(r_p/r_s\right)$ ratio of 0.7938. The optimized ratios are used to develop an inertial type non-linear energy harvesting device. The structure of the non-linear harvester is same as the linear one except two stationary magnets are added at the top and bottom of the harvester that act as a non-linear spring. The non-linear harvesting device is tested and the power density of the system is determined to be 2.738e-2 W/cm^3. The non-linear harvester was tested at acceleration level of 1g and it was determined that the harvester worked best at

natural frequency of 8.66 Hz. The maximum power produced was 38.1 mW. The non-linear type of harvester is easy to assemble and optimize to match ambient natural frequency of numerous vibrating systems. Two frequency tuning methods are looked at for the non-linear energy harvesting system. One is by changing the magnetic air gap and the second is by changing the thickness of the stationary top and bottom magnets. It is determined that changing magnetic air gap is more effective at tuning for a range of natural frequencies. For applications where the natural frequency of the system doesn't exist, such as buoys and beacons at sea, the linear energy harvester works best. For applications where the system vibrates at a certain natural frequency, the non-linear harvester should be used.

Finally, this thesis is concluded with a discussion on the electromagnetic micro-harvester and some suggestions for further research on how to optimize and extend the functionality of the energy harvesting system.

Acknowledgements

I would like to thank my supervisor, Professor Behrad Khamesee for his technical guidance, support and encouragement during my research.

I would also like to thank Professor William Melek and Professor Eihab Abdel-Rahman for reviewing my thesis. I would like to acknowledge Professor Armaghan Salehian for providing testing shaker as well as Mohammad Ebrahim for showing me the functionality of the equipment. To the student machine shop technicians Phill Laycock and Andrew Urschel for providing me with guidance and technical support for prototyping and manufacturing of my hardware.

I would also like to express my gratitude to my colleagues Mohammad Mashagbeh, Roberto Riberio, Ehsan Asadi and Xiaodong Zhang in the Maglev Microrobotics Laboratory who provided me with helpful suggestions.

I am forever grateful to my parents, for teaching me respect and hard work. I wouldn't have come this far without their support, guidance and love. I would also like to thank my friends for constant motivation and support.

Dedication

I would like to dedicate this thesis to friends and family who have always supported and believed in me. It is because of your support and inspirations that I am able to successful complete my journey through difficult times.

Table of Contents

List of Figures

List of Tables

Nomenclature

Symbol	Units	Variable
B_m	T	Flux density of the magnet
B_s	T	Flux density of the stator
A_s	m^2	Cross sectional area of the stator
A_m	m^2	Cross sectional area of the magnet
B_g	T	Flux density in the air gap
A_g	m^2	Lateral area of the air gap
B_p	T	Flux density in the iron pole
A_p	m^2	Lateral area of the pole
r_p	m	Radius of the magnet and iron pole
r_m	m	Radius of the mover
r_t	m	Outside radius of the stator
r_s	m	Inside radius of the stator
τ_p	m	Iron pole thickness
B_{rem}	T	Remnant flux density
τ_m	m	Magnet thickness
μ_{rec}	-	Recoil permeability
μ_r	-	Relative permeability of Iron
μ_0	$H \cdot m^{-1}$	Permeability of free space ($4\pi \times 10^{-7}$)
v	m/s	Velocity of the mover
N	-	Number of turns in coil
F_{em}	N	Electromagnetic force
D_{em}	$N \cdot s/m$	Electromagnetic damping
P_e	W	Total Extracted Power
V_{ab}	V	Open loop Voltage

R_L	Ω	Load Resistance
R_C	Ω	Coil Resistance
m	kg	Mass of Mover
k	N/m	Spring Stiffness of Linear Spring
$Y(t)$	m	Sinusoidal input to the base
$X(t)$	m	Displacement of the base + mover
$Z(t)$	m	Displacement of mover
L_C	H	Inductance of coil
D_{mech}	$N \cdot s/m$	Mechanical parasitic damping
D_{Wire}	m	Diameter of magnet wire
L_w	m	Total length of magnet wire for all coils
r_{wire}	m	Radius of magnet wire
l_m	m	Length of magnet and iron pole
l_s	m	Length of stator
L_T	m	Total length of non-linear energy harvester
L_s	m	Length of stationary magnet
L_g	m	Length of gap
L_m	m	Length of stator
F_r	N	Total restoring force
F_t	N	Force exerted by top magnet
F_b	N	Force exerted by bottom magnet
F_g	N	Gravitational force acting on the mover
k_x	N/m	Non-linear spring stiffness term

Chapter 1

Introduction

Increase in energy consumption has facilitated research into renewable energy sources that are found in the environment. Thus far numerous sources have been investigated such as solar, wind, mechanical vibrations and noise to name a few. Harnessing energy from these sources is referred to as ambient energy scavenging. Sources such as solar and wind energy are usually used for large scale applications for harnessing large amount of power. Sources such as mechanical vibrations and noise have lower power capabilities, however they are just as important sources as solar or wind energy. Mechanical vibration is one of the most common sources of energy as it can be available almost anywhere from sources such as bridge, human locomotion and vibrating and rotating machinery. In recent times, mechanical vibrations have seen a lot of research and growth in wireless sensor networks (WSN) field. The power requirements of sensors have decreased as technology has developed over the year. For this reasons the requirement of self-sustaining wireless sensor has increased dramatically. Currently, battery powered energy sources are used to power low powered electronics. However, batteries can only carry finite amount of energy and so it needs constant replacement. Battery replacement can become a huge drawback where electronics are placed in hazardous environment or unreachable places. For this reasons self-sustaining harvesting devices have been sought after to provide an infinite amount of energy from the environment and convert it to useful electrical energy. The benefits of self-sustaining sensors include minimal maintenance, increased reliability and long lasting. There have been three most common types of harvesting devices for converting mechanical vibrations to useful electrical energy. Piezoelectric, electrostatic and electromagnetic harvesters have been developed to be integrated with sensor to make the system self-sustaining. As vibrational energy is spread through the entire frequency spectrum, many different variations of energy harvesters have been developed to target certain frequency or application.

The working mechanism as well as some of the most common development in vibrational energy harvesting systems discussed here is comprised of piezoelectric,

electrostatic and electromagnetic energy harvester. Before looking at the current harvesters available it is important to discuss the working mechanism of each type of harvester.

Piezoelectric harvesters generate energy when a piezoelectric material is strained by vibrations. Separation of charge occurs when deformation takes place to produce electric field. Two most common modes used for harvesting is mode 31 and 33. Mode 31 is distinguished when the electric field created is in perpendicular direction from the strain direction whereas mode 33 is parallel to the strain direction. Piezoelectric energy harvesters are cantilever type with additional mass added at the tip to dampen the vibration. The voltage generation for piezoelectric harvester is usually higher than that of electromagnetic and electrostatic harvesters but piezoelectric harvesters suffer from high operating frequency.

Electrostatic harvesters generate voltage when a variable capacitor is charged and the plates are moved with respect to each other due to vibration. Separation in capacitor plates causes energy to be transferred from mechanical energy to electrical energy and the energy can be harvested when plates come together. The most attractive feature of electrostatic harvester is that they can be integrated with low power integrated circuits (IC) for self-sustaining operation. For electrostatic harvesters to work there has to be initial charge placed on the capacitor plates. Usually this requires very high voltage which is one of the drawbacks of this type of method. The voltage generation is usually quite high but it suffers from low power density. Electrostatic harvesters are usually designed for harvesting voltage at lower frequencies.

Electromagnetic energy harvesters work on the principles of Faraday's law. Back emf is produced in the coils when it cuts through the magnetic field generated by the moving magnets. Electromagnetic harvester can be planar or tubular but tubular designs are of preferred choice as they are more efficient in voltage generation. Electromagnetic harvesters of tubular design can vary as the magnet can be moved relative to the stationary coils or the coils can be moved relative to the stationary magnet. It has been shown that electromagnetic harvesters with moving magnets produce higher power as it causes complete flux reversal within the system to increase the voltage generation [1]. Moving magnet type harvester is

also easy to construct and is very rugged compared to piezoelectric or electrostatic harvesters. The power density of electromagnetic harvester can vary depending on the size, but is usually lower than of piezoelectric harvesters. Electromagnetic harvesters are usually of micro and macro scale and the operating frequency range can vary from few hertz to couple of hundred hertz.

Some researchers have also developed hybrid harvesters that take advantage of two harvesting methods. Hybrid harvesters usually are of cantilever piezoelectric beam with magnet at the tip. The efficiency of the system increases when two methods are combined. Various piezoelectric, electrostatic, electromagnetic and hybrid harvesters developed by researchers and research institutions will be looked at in detail in Chapter 2.

1.1 Research Motivation

This research is motivated to develop an electromagnetic energy harvester that is optimized in terms of power to volume ratio. The harvester should also be capable of working at natural frequencies that are in the range of 0-35 Hz. There are many applications which work at very low frequencies such as human locomotion and outdoor power equipment such as Lawnmower, Snow Blower and Pressure Washer. Car and bridge vibration also fall within the frequency range of 0-35 Hz. Electromagnetic energy harvester is developed for the use of power equipment for the purposes of obstacle detection, fuel consumption and vibration monitoring. This thesis aims to:

- Investigate and develop an linear efficient micro scale electromagnetic harvester of AA battery size
- Optimize the linear energy harvester for maximum peak performance using Finite Element Analysis (FEA) software Comsol.
- Extend linear harvesting system to non-linear harvesting system to work as an inertial harvester by the use of stationary top and bottom magnets that act as a non-linear magnetic spring.

- Experimental testing to verify the design and comparison of the developed harvesters with those available in the literatures for performance evaluation.

1.2 Thesis Outline

Chapter 1 presents a general overview of the energy harvesting system and the types of vibrational kinetic energy harvesting systems available.

Chapter 2 provides a literature review of vibrational kinetic energy harvesting devices. Piezoelectric, electromagnetic and electrostatic energy harvesters developed by researchers have been discussed in depth. The motivation behind the thesis is discussed along with the goals that the thesis will achieve.

Chapter 3 provides a detailed analysis of linear electromagnetic energy harvesting system. Theoretical model for the mechanical and electromagnetic system is developed and the energy harvester is optimized using finite element analysis software. This section also described the experimental setup and results with detailed analysis.

Chapter 4 describes the development of optimized energy harvester. Magnet at the top and bottom are added to convert the optimized energy harvester into non-linear harvester. Theoretical model for the non-linear system is described and FEA has been used to further validate the theoretical model. The non-linear energy harvesting system is experimentally tested and tuned to work at various natural frequencies. The results are discussed in greater detail and the theoretical model is validated.

Finally, the thesis concludes with design and performance of energy harvesting systems and potential improvements that can be made to the system in chapter 5. Future work to build on the current energy harvester is discussed.

Chapter 2

Literature review and Research Motivation

2.1 Energy Harvesting Devices

2.1.1 Piezoelectric

Many piezoelectric energy harvester developed are of cantilever type with added mass at the tip for increasing the damping and to reduce the working natural frequency of the system. Various approaches have been developed by many researchers around the world in the field of piezoelectric device for maximum power and current generation.

Researchers at University of Southampton[2] have devised a thick film piezoelectric energy harvester based on screen printing method. The harvester is made of 316 steel beam substrate of 0.1 mm thickness. Dielectric material of 20 μm thick has been printed on both side of the steel beam while a thick film piezoelectric (PZT 5H) and electrode layers are deposited using multiple printings on top. The harvester was tested on an electromagnetic shaker and it was determined that at 0.9 mm displacement amplitude, the harvester was capable of generating 2 μW of power at an optimal load resistance of 333 kΩ. The maximum voltage that the harvester was capable of generating was around 1.2 V.

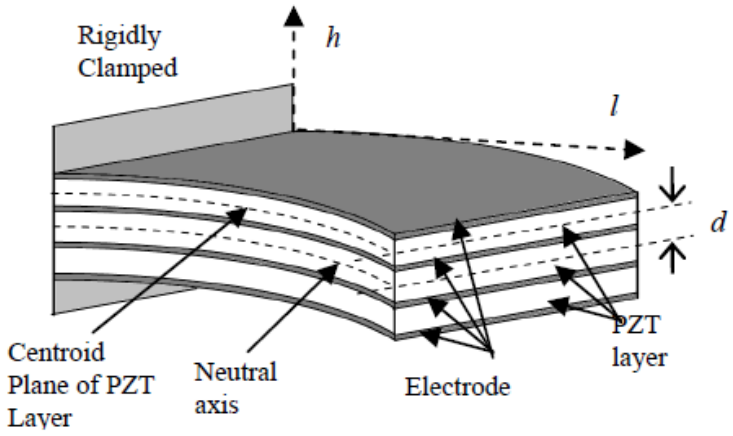

Figure 2-1: Multimorph PZT cantilever beam [3]

Similar work by different researchers at University of Southampton has been done to develop a multimorph cantilever harvester in a free standing form for the use in silicon technology [3]. Authors have stated that the piezoelectric harvesters developed in [2] use a substrate of steel which acts as a support and does not contribute to any electrical conversion. The multimorph beam consist of three Lead Zirconium Titenate (PZT) layers of 40 μm thickness sandwiched in between four silver/palladium (ag/pd) electrodes of 12 μm as seen in Figure 2-1. The paper investigates the multimorph structure that is polarized in series and parallel configuration. Tests are conducted to determine the power and voltage output of the structure on a shaker. It is determined that the series configuration produces 1.3 V at load resistance of 38 kΩ which translates to a power output of about 42 μW compared to only 29 μW for parallel configuration. During testing it is determined that series polarized structure is more suitable for energy harvesting purposes while the parallel polarized structure is preferred for actuator applications.

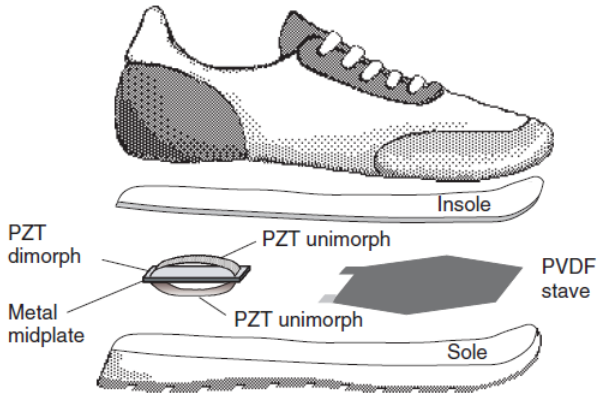

Figure 2-2: Insole Piezoelectric Energy Harvester [4]

Research has been conducted in MIT Media lab for harnessing human walking motion using Piezoelectric material for powering radio frequency identification tags (RFID) [4]. The paper looks to harvest energy from foot strike to the ground and bending near ball of the foot. A Flexible multilaminar polyvinylidene fluoride (PVDF) is used to harness energy near ball of the foot as shown in Figure 2-2, while a two curved PZT unimorphs are bonded to mid plate is used to harness energy from foot strike. The PVDF stave and PZT dimorph are tested on Nike sneakers and U.S Navy boots to power a 12 bit wireless identification

code. During testing it is determined that the PVDF state produced an average power of 1.3 mW at walking pace of 0.9 Hz at 250 kΩ load resistance while the PZT dimorph produced average of 8.4 mW power at 500 kΩ. The large power production in PZT material at the heel is due to greater bending due to heel strike. Many other applications are presented for this type of harvester such as pagers, health monitors and emergency receivers but were not physically tested.

A MEMS based piezoelectric harvester has been proposed by [5] to convert ambient vibrations to electrical energy. The harvester consists of a PZT composite cantilever beam with nickel mass at its tip. MEMS manufacturing techniques have been used to manufacture and measure the performance of the harvester. The composite cantilever is made of platinum /titanium electrode and PZT material that exploit 31 excitation mode rather than 33. Mode 31 is believed to give better performance for MEMS device. The harvester is capable of producing 2.16 μW of power at load of 21.4 KΩ and 1g acceleration at its resonance frequency of 608 Hz. It is assumed that 31 excitation mode is better than 33 but it has not been tested to fully to verify the assumption that has been stated in the paper.

A new piezoelectric-magnetostrictive harvester has been proposed by [6] to increase the efficiency of energy harvesting systems. PZT of 0.5 mm thickness was sandwiched in between two magnetostrictive Teflon-D layers of 1.5 mm thickness. The Teflon layers and PZT is cured using a silver epoxy. The harvester is proposed for low frequency wireless system based on magnetoelectric effects. Testing showed that the system is capable of generating 285 V peak to peak when the distance between the magnet producing the magnetic field is 1 mm from the laminate. The power output of the harvester can range from 10-80 μW at low frequencies.

Piezoelectric harvester developed so far employ the 31 excitation mode which is distinguished by electric field in perpendicular direction to the strain direction. However, mode 33 is used which is parallel direction of magnetic field to strain direction. Authors in [7] have developed a piezoelectric harvester that works on mode 33 that is capable of generating 20 times higher voltage than the mode 31. The harvester is characterized by testing at various frequencies. The tip displacement was determined with a laser vibrometer.

Testing revealed three resonant modes at 13.9 kHz and 48.5 kHz which corresponds to bending modes while the torsional mode occurs at 21.9 kHz. The harvester was excited at its first resonant frequency of 13.9 kHz which indicated that the maximum voltage generated was 3V. The maximum continuous electrical power delivered to a load of 5.2 MΩ was 1 μW. The corresponding energy density of the harvester determined was 0.74 mW h/cm^2.

2.1.2 Electrostatic

Very first electrostatic energy harvester in literature was introduced by [8] which employs MEMS technology to create a variable capacitor for energy generation. The capacitors top and bottom plate is made of silicon wafer separated by silicon dioxide. Silicon acts as insulator to form parasitic capacitor between the two plates [8]. The overall MEMS harvester is shown in Figure 2-3 and it consists of floating mass, spring and two interlocked combs. The operating frequency is determined to be 2.52 KHz. The two capacitor plates move together and separate to create variable capacitance. The charge in capacitance of the system has to be maximum for full energy transfer. The devices is tested and it is reported that 8.6 μW of power is available.

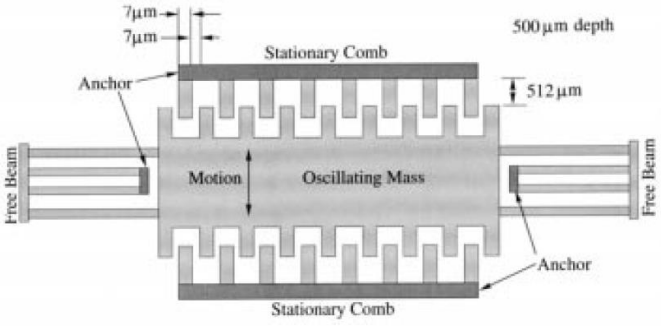

Figure 2-3: MEMS electrostatic harvester [8]

A variable capacitance electrostatic generator has also been developed by [9] for it to be used in driving a cardiac pacemaker. The generator uses ventricular walls as a vibrating source because it has the largest motion compared to other organs in the human body. The frequency of movement of the ventricular walls is found to be 1 to 2Hz so the authors have tried to develop a generator that works at extremely low frequency. Honeycomb type variable

capacitor is developed by folding pair of long electrodes made of polyester film [9] and glued together with adhesives as seen in Figure 2-4.

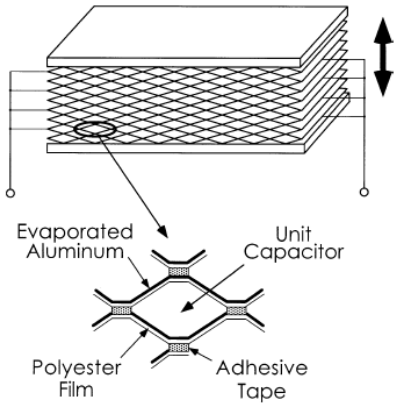

Figure 2-4: Honeycomb electrostatic generator [9]

The total amount of cells incorporated within the honeycomb structure amounts to 1000 and the structure is enclosed with acrylic boards. The resonant frequency of the harvester is 6 Hz which is outside the working range of the ventricular walls but is still capable of generating energy at low frequencies. The generator was capable of generating 36 μW of power with a canine heart which is enough to power a cardiac pacemaker. The authors have proposed MEMS fabrication of this technology to be used as a generator.

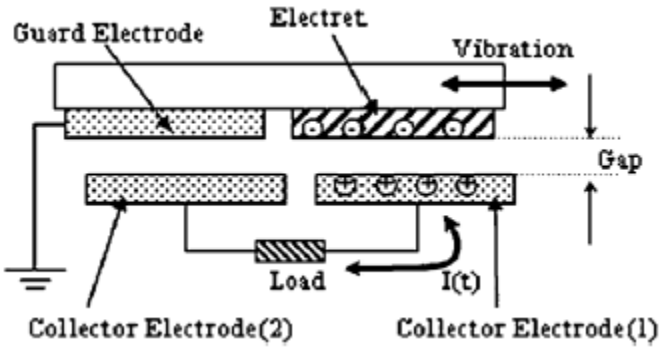

Figure 2-5: New Electret electrostatic harvester [10]

Electrostatic harvesters are capable of harvesting energy for low frequency applications which makes it suitable for harvesting human motions. Authors in [10] have developed an electrostatic generator that is capable of harvesting energy at 2 Hz. The harvester developed consists of a new dielectric silicon dioxide electret structure, collector

electrode, mover and silicon substrate. Charge is induced in collector electrode 1 as the electret is aligned with the electrode 1. As the electret moves towards electrode 2, the charge from electrode 1 is transferred to electrode 2 through the load connected with the two collector electrodes. At 2 Hz and 0.4 g's , the maximum power output developed is 40 μW in external load of 7 MΩ.

2.1.3 Electromagnetic

Authors in [11] have devised a wireless condition monitoring sensor system (ACMS) for industrial air conditioning unit and an air compressor unit. The unit is used to transmit vibration data from the air conditioner (AC) and air compressor wirelessly for continuous monitoring of its vibration levels. The ACMS is powered by an electromagnetic harvester that is capable of harvesting electrical energy by converting vibration from the A.C unit. The electromagnetic harvester devised has a volume of 150 mm^3 and is capable of generating 58-120 μW at acceleration levels of 0.6-1.7 m/s^2 at frequency of 52 Hz power into a load resistance of 15 kΩ.

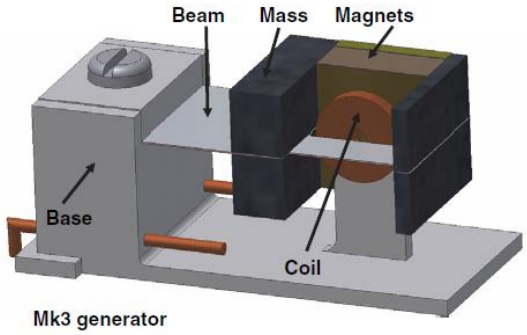

Figure 2-6: MK3 Electromagnetic harvester with cantilever beam [11]

The electromagnetic harvester described in [11] consists of four Neodymium Iron Boron (NdFeB) magnet mounted to the beryllium copper beam to obtain low resonant frequencies and can be seen in Figure 2-6. The stationary coil is made of 12 μm cooper wire consisting of 2800 turns. Zinc coated mild steel is placed besides the magnet to couple the magnetic field between top and bottom magnets. Four tungsten masses have been added as well for achieving desired frequency. The generated voltage from the harvester is insufficient to power microcontrollers so the voltage has to be rectified and stepped up to 2 V for it to be

usable. As a result, a voltage multiplier circuit is used to extract power from the generator by increasing the damping of the system. The efficiency of the system is claimed to be 53% which is greater than piezoelectric generator (35%). The system is fully autonomous and is capable of transmitting acceleration data every 3 seconds when the vibration of the unit is at 0.6 m/s^2. The data can only be sent every 3 seconds because sufficient charging needs to take place for stable operation of the system even when the vibration is low.

Electromagnetic MEMS energy harvester has been developed in [12] for distributed sensor systems. The MEMS harvester is used to convert vibrational kinetic energy to electrical energy for it to be used in low-power integrated circuits or micro sensors. The author demonstrates micromachining techniques to produce an efficient generation and ability to mass produce at low cost for it to be commercially available. The harvester consists of a spring attached to a NdFeB magnet and a base. Voltage is induced in the coil when magnet moves relative to the coil. Zig-zag patterned spring and spiral spring has been tested to demonstrate that when the spring is made of brass and copper, a resonant frequency of 10 Hz can be achieved. Spiral spring is chosen as it has lower spring constant and stress concentration to obtain large displacements. Benefit of the spring system is that it is capable of transferring vertical input vibrations to make the mass vibrate horizontally for higher voltage output. Total volume of the energy harvest is 1 cm^3 that is capable of producing RMS power of 830 μW of power at load resistance of 1000 Ω driven at input frequencies of 60-110 Hz. Voltage was stepped up to 2-4 V by a quadrupler circuit to drive an Infrared (IR) transmitter and Radio frequency (RF) Transmitter. It was demonstrated that the harvester was capable of producing enough power for the IR and RF transmitter to work. Author hopes to use this sensor for the distributed sensor systems as power requirements in low powered electronics will decrease due to advancement in technology.

Micromachining and micro plating techniques have been utilized for developing MEMS electromagnetic harvester to reduce the volume. Researchers from Researc Institute [13] used silicon micromachining and micro plating techniques to develop a harvester capable of harvesting energy at frequencies of 100-300 Hz. The harvester consisted of NdFeB magnet attached to a nickel spring and stationary top and bottom coil. It is claimed

that the output performance of energy harvester is increased by lowering air damping by creating air channels in silicon frame of the harvester. The harvester is capable of producing 142.5 mV at resonant frequency of 280 Hz when the input vibration is 10 m/s^2. The maximum power obtained is about 17.2 μW at load resistance of 81 Ω. Application for this harvester is belied to be in intelligence monitoring, health care and automotive industry but it has not been tested on any application thus far.

An electromagnetic harvester developed at University of South Hampton [14] has been tested on automotive applications as shown in Figure 2-7. Two miniature micro generators of volume 0.84 cm^3 and 3.15 cm^3 have been developed.

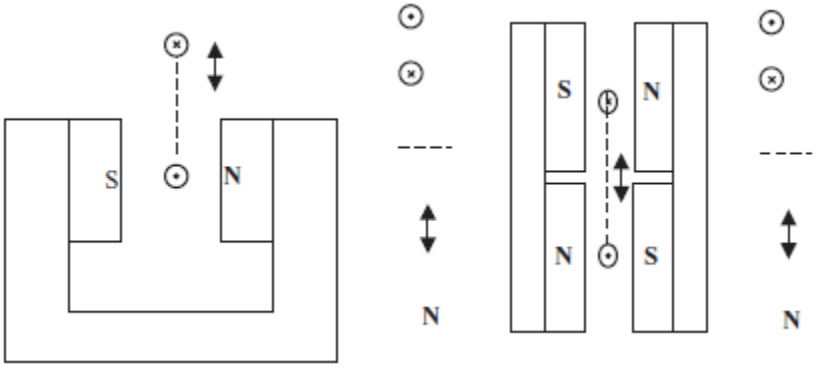

Figure 2-7: Miniaturized energy harvester (Prototype A on left) [14]

Prototype A consists of NdFeB magnet with a moving coil attached to an etched stainless steel cantilever beam. Prototype A is capable of generating 37-180 μW at 0.36 mm beam deflection at frequency of 322 Hz when an optimum load resistance of 0.6 Ω is connected. A major drawback to prototype A is low voltage is produced (9 mV) and manufacturing of coil was a big issue. Prototype B in Figure 2-7 is developed to overcome these issues that prototype A faced. Prototype B consists of four magnets to increase the voltage generation of the harvester to 1 mV. Harvester was placed and tested on a car engine. The harvester was capable of harnessing 157 μW of power over the course of the test when the car was drove around at a 25 km/hr speed.

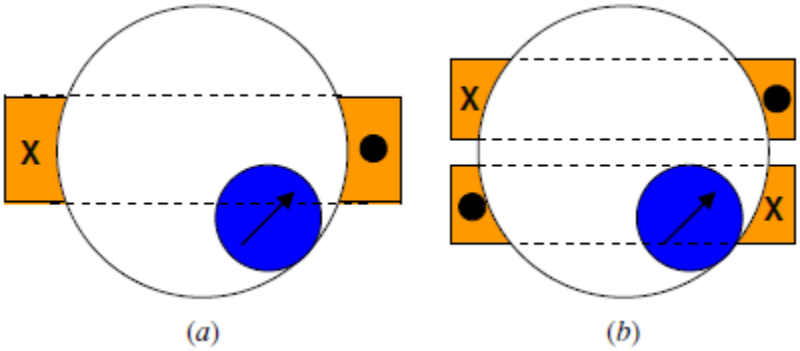

Figure 2-8: Spherical rolling magnet [15]

Another interesting energy harvester has been developed by Bowers and Arnold based on rolling of magnet inside copper coils for harvesting energy from human locomotion [15]. Human locomotion such as running, walking and breathing all dissipate vibrational kinetic energy which can be used to harness useful electrical energy for the use of human implanted medical devices. Some of the common medical devices that can be powered include hearing aids, pacemakers and other external biomedical devices to name a few. One of the biggest challenges of harvesting human locomotion is that the vibrational frequency is very low (1-10 Hz) and unpredictable. For this reason a non-resonant energy harvester is developed consisting of unidirectional magnetized spherical magnet rolling inside a hollow spherical cavity as seen in Figure 2-8. The coil is wrapped around the spherical cavity around the equator for the first prototype. The second prototype consists of two coils which are counter wound. Coils consisting of 400,600 and 800 turns were tested while changing the magnetic ball to outer cavity ratio. The device was tested by a person walking at a speed of 4 km/hr and running at 14.5 km/hr. It was determined that the power densities of 0.03-0.5 mW/cm^3 were obtained with voltage output consisting of 80-700 mV.

Similar harvester proposed by [15] has been developed by University of Barcelona [16] which consists of a spherical rotating magnet. The harvesters intended use is for maritime systems such as buoys, beacons and autonomous equipment on ports and fishing exploitations. It is also intended for human locomotion, bicycles and small vehicle motion. The harvester is of non-resonant type and is capable of harvest energy for low frequency high amplitude vibrations.

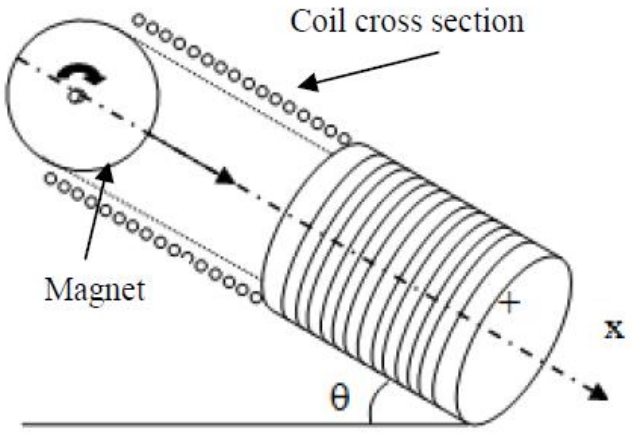

Figure 2-9: Harvester with spherical rolling magnet [16]

The device is capable of turning small inclinations in buoys and converting it to large displacements for maximum power generation as compared to cylindrical magnets. The device consists of a 2 cm diameter spherical rolling magnet of diametrical magnetization. The magnet is allowed to rotate and slide inside a tube as seen in Figure 2-9. Eight coils are wound from a Copper wire of 100 μm in diameter and consist of 3000 turns. All the coils are either connected in series or in phase. Authors have claimed that the harvester is capable of achieving power density of 1.5 mW/cm^3. One of the drawbacks of this type of spherical rolling magnet is that the magnet would orient itself toward zero flux position. In this position the power and voltage output would be zero. A ring is placed on the magnet so that the magnet doesn't orient itself into zero flux position. The harvester is claimed to be extremely robust, easy to manufacture and can work in wide variety of applications.

One of the most common problems with energy harvesting systems is that they work at only one frequency which is at the devices resonant frequency. Same harvester performance drops considerably when excited outside of its natural frequency. Vibrational kinetic energy is usually spread through the entire frequency spectrum so one of the main challenges has been to develop a multi frequency harvester. A multi frequency electromagnetic harvester has been proposed by [17] as seen in Figure 2-10.

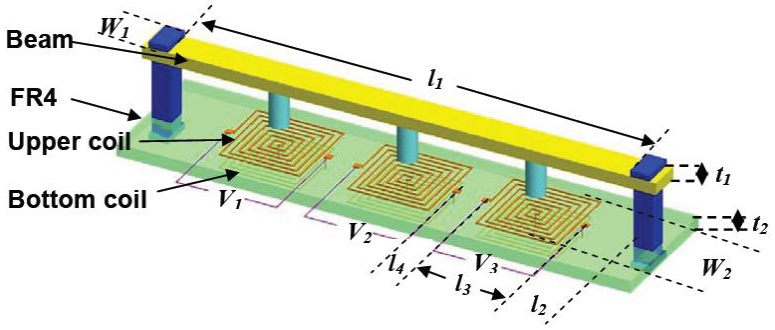

Figure 2-10: Multi frequency energy harvester [17]

Previously reported energy harvester are silicon based that are not always cost effective. Harvester proposed in Figure 2-10 is polymer based solution which uses Printed Circuit Board (PCB) technology to fabricate low cost copper coils. Harvester consists of three NdFeB magnets attached to a polymer structure that is capable of vibrating at different modes, while the bi-layered copper coils are held stationary on a supported acrylic beam. Several characteristics of a the harvester are studied for performance optimization such as increasing vibration amplitude, changing coil turns and decreasing gap between magnet and coils. Experimental tests showed that the harvester was capable of harvesting energy at three frequencies of 369 Hz, 938 Hz and 1184 Hz. Maximum power output generated was 1.157 μW at 14 μm amplitude and 0.4 mm gap between the magnet and coils. The intended application is unclear, however the harvester is a low cost solution that is capable of harvesting energy at three different vibration frequencies.

Harvester in Figure 2-11 consists of a moving magnet and two stationary magnets at the top and bottom. Top and bottom magnets are oppositely attracted to the moving magnets to create a magnetic spring. Moving magnet dimensions as well as coil dimensions are optimized for maximum power generation. Top and bottom stationary magnets have different dimensions to compensate for gravitational forces acting on the moving magnet. Dimensions of the bottom magnet are 2x2 mm^2 while the top is 1x1 mm^2 and the optimized middle magnet dimension is 6x14 mm^2. Optimized AA battery size harvester is capable of producing power of 53.5 mW at load resistance of 97 Ω with input displacement of 0.5 mm at 8.1 Hz. The proposed harvester is more rugged, low cost and works at lower frequencies as compared to previous harvester described.

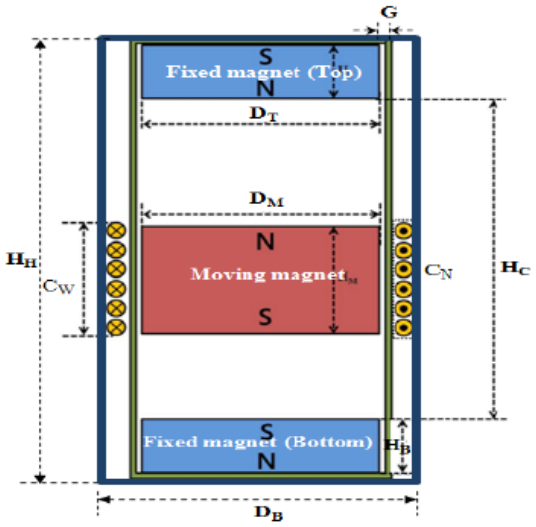

Figure 2-11: Magnetic Spring Energy Harvester [18]

It is worth mentioning that all the energy harvesting solutions covered so far are based on only one harvesting mechanism. To improve the performance of the energy harvesting systems, researchers have combined multiple harvesting methods. Challa, Prasad and Fisher [19] have proposed a combined piezoelectric-electromagnetic energy harvesting system in Figure 2-12.

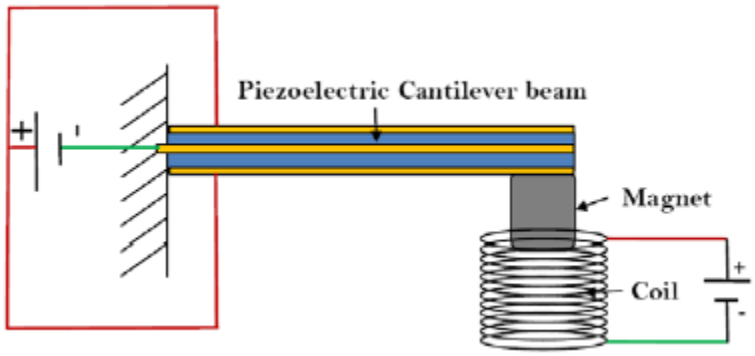

Figure 2-12: Coupled piezoelectric-electromagnetic harvester [19]

A piezoelectric cantilever beam is made of two piezoelectric layers sandwiched in between two electrodes in parallel configuration consisting of NdFeB magnet at its tip. Total damping in the system is increased by adding a mass. Additional of extra mass decreases the natural frequency of the system as well as the power output from the piezoelectric beam. The device should have electrical damping higher than mechanical damping to see higher power outputs

of the combined system. Authors have demonstrated that the total electrical damping is the sum of electrical damping from piezoelectric and electromagnetic components. On the other hand, total power output is not sum of two optimized system as the increase in damping reduces the amplitude of the piezoelectric cantilever beam. To demonstrate this concept, piezoelectric and electromagnetic systems were tested alone at first and then compared with the combined piezoelectric-electromagnetic system. Total power output of the coupled device was 332 μW as compared to 257 μW from the piezoelectric harvester and 250 μW from electromagnetic harvester. Comparing the standalone systems, the combined system had 30% increase in power output at its operating frequency of 21.6 Hz.

Chapter 3

Linear Energy Harvesting Device

This chapter presents the development of a linear electromagnetic energy harvesting system. The developed energy harvesting system is a force based that can be used under any excitation frequency for low to high amplitude applications. Section 3.1 covers the working theory of the electromechanical components of the harvester while section 3.2 will cover the design aspect of the energy harvesting system. For improvement of the harvesting system, Comsol FEA analysis has been used and will be presented in section 3.3. Section 3.3 also covers the testing procedure used to test the linear harvesting system.

3.1 Theory

3.1.1 Mechanical System Modeling

In this section a complete mathematical model of electromagnetic energy harvester is developed along with the mechanical model. Mechanical system of the energy harvester can be described as a second order single degree of freedom mass spring damper system developed in Figure 3-1. The governing equation of motion of the system is described as:

$$m\ddot{z} + D_{mech}\dot{z} + kz = -m\ddot{y} \tag{3-1}$$

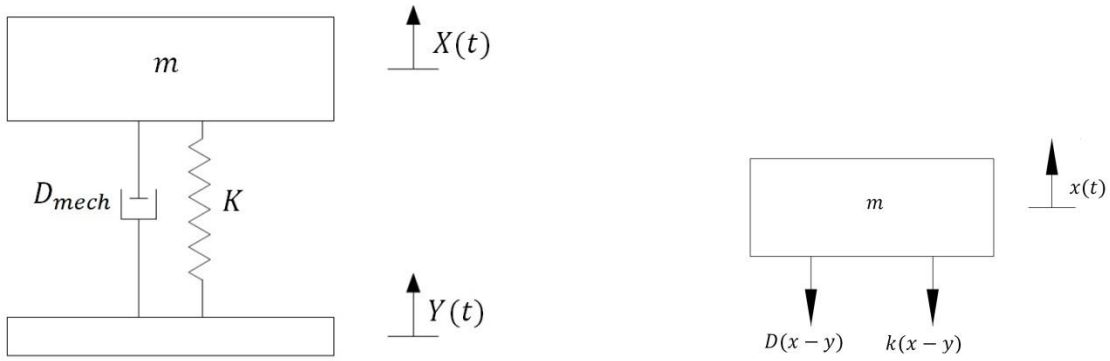

Figure 3-1: Single Degree of Freedom

The single degree of freedom consists of a moving base, moving mass (m), spring with stiffness (k), and mechanical damping (D_{mech}). The system oscillates when an input function

of $Y(t)$ is applied to the base. $X(t)$ is movement of the mass and the base so the movement of the mass alone can be described as $Z(t) = X(t) - Y(t)$. Oscillations of the system are highly dependent on the mass, spring stiffness and damping coefficient. Linear energy harvesting system does not consist of a spring so the working natural frequency of the system in not present. However, later in chapter 4 the non-linear system discussed will consist of magnetic springs. Mechanical modelling is valid for both linear and non-linear systems as they work on the same principles.

In energy harvesting systems, the moving mass is called the mover that consists of magnet and iron pole while the base is called the stator consisting of coil, outer iron shell and coil holder. As the system vibrates, the mover translates up and down relative to the coil to induce emf within the coils. The emf generated within the coils is developed in section 3.1.2 where the electrical and electromagnetic model is developed.

3.1.2 Electrical and Electromagnetic Model

Analysis of electromagnetic model is based on the circuit shown in Figure 3-2 while the electrical model is based on the electrical circuit shown in Figure 3-3.

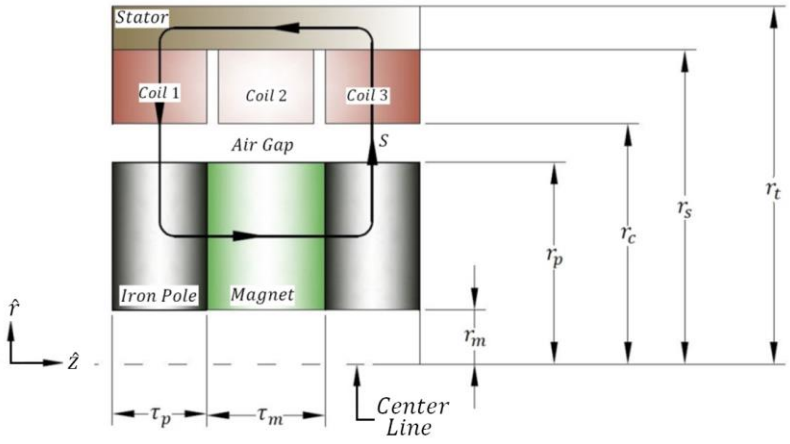

Figure 3-2: One stack of magnet and iron pole configuration [20]

Electromagnetic model consists of coils, magnet, iron pole and the outer iron shell. Electromagnetic model is derived based on the assumptions that there is no leakage of flux in the system. Magnetic field in the iron poles and stator is purely axial while the magnetic field

in the coils is purely radial [1]. In a closed loop circuit, conservation of flux is defined in (3-2). By applying conservation of flux to the geometry in Figure 3-2, relationship between magnet and the stator can be formed as shown in (3-3). Similarly, magnet to gap and magnet to iron pole relationship is defined in (3-4) and (3-5).

$$\oint B \cdot dA = 0 \tag{3-2}$$

$$B_m A_m - B_s A_s = 0 \tag{3-3}$$

$$B_m A_m - B_g A_g = 0 \tag{3-4}$$

$$B_m A_m - B_p A_p = 0 \tag{3-5}$$

Equation (3-3) , (3-4) and (3-5) can be rearranged to determine the flux density of the stator, gap and the pole as a function of magnets flux density.

$$B_s = \frac{B_m A_m}{A_s} \Rightarrow B_s = \frac{B_m \left(r_p^2 - r_m^2\right)}{\left(r_t^2 - r_s^2\right)} \tag{3-6}$$

$$B_g = \frac{B_m A_m}{A_g} \Rightarrow B_g = \frac{B_m \left(r_p^2 - r_m^2\right)}{2 r \tau_p}, \quad r_p < r < r_s \tag{3-7}$$

$$B_p = \frac{B_m A_m}{A_p} \Rightarrow B_p = \frac{B_m r}{2\tau_p}, \quad r_m < r < r_p \tag{3-8}$$

Air gap flux density needs to be known for power dissipation in coils and damping coefficient estimations. (3-7) is used to determine the air gap flux density but the magnetic flux density needs to be determined as gap flux density is related to magnets flux density by (3-7). Magnetic flux density can be determined by applying the ampere's law to the magnetic circuit loop S shown in Figure 3-2. Just as the sum of all voltage around electric circuits in closed loop is zero, the sum of magnetomotive force around a closed loop in magnetic circuit must also equal to zero as shown in (3-9).

$$mmf = \oint H \cdot dl = 0 \tag{3-9}$$

$$\frac{\left(B_m - B_{rem}\right)\tau_m}{\mu_{rec}} + 2\int \frac{B_p}{\mu_0 \mu_r} dl + 2\int \frac{B_g}{\mu_0} dl + \frac{B_s\left(\tau_p + \tau_m\right)}{\mu_0 \mu_r} = 0 \tag{3-10}$$

$$\frac{\left(B_m - B_{rem}\right)\tau_m}{\mu_{rec}} + \frac{B_m\left(r_p^2 - r_m^2\right)}{\mu_0 \tau_p}\left[\frac{1}{2\mu_r} + ln\left(\frac{r_s}{r_p}\right) + \frac{\tau_p\left(\tau_p + \tau_m\right)}{\mu_r\left(r_t^2 - r_s^2\right)}\right] = 0 \tag{3-11}$$

Substituting (3-6), (3-7) and (3-8)into (3-10) gives **(**3-11). The flux density of the magnet can be derived by rearranging **(**3-11). By substituting **(**3-11) into (3-7), the gap flux density can also be found.

$$B_m = \frac{B_{rem}}{\left(1+\frac{\mu_{rec}\left(r_p^2-r_m^2\right)}{\tau_m\mu_0\tau_p}\left[\frac{1}{2\mu_r}+ln\left(\frac{r_s}{r_p}\right)+\frac{\tau_p\left(\tau_p+\tau_m\right)}{\mu_r\left(r_t^2-r_s^2\right)}\right]\right)} \tag{3-12}$$

$$B_g = \frac{B_{rem}\left(r_p^2-r_m^2\right)}{2r\tau_p\left(1+\frac{\mu_{rec}\left(r_p^2-r_m^2\right)}{\tau_m\mu_0\tau_p}\left[\frac{1}{2\mu_r}+ln\left(\frac{r_s}{r_p}\right)+\frac{\tau_p\left(\tau_p+\tau_m\right)}{\mu_r\left(r_t^2-r_s^2\right)}\right]\right)} \tag{3-13}$$

Emf is induced within the coils as the magnet moves relative to the coil. Induced emf in the coil can be determined from Faraday's law.

$$emf = -\frac{d\Phi}{dt} \Rightarrow -\frac{d}{dt}\int B_g \cdot ds \Rightarrow V_{ab} = \frac{NB_m\left(r_p^2-r_m^2\right)\pi v}{\tau_p} \tag{3-14}$$

Power can be extracted when an external load is connected to the energy harvester. External load will cause a current to flow within the coils to produce an opposing field that was created by permanent magnets according to lenz law [11]. Electromagnetic force will be produced as a result of the interaction of two opposing fields. The electromagnetic force can be characterized as:

$$F_{em} = D_{em}v \tag{3-15}$$

The power extracted is defined in (3-16) as power extracted is a function of electromagnetic force and velocity of the mover.

$$P_e = F_{em}v \tag{3-16}$$

The extracted power is dissipated in the load and the coil as shown in electrical circuit developed in Figure 3-3. The governing equation for the electrical circuit is developed in (3-17) and can be further simplified to (3-18) because the inductance is negligible due to small winding area.

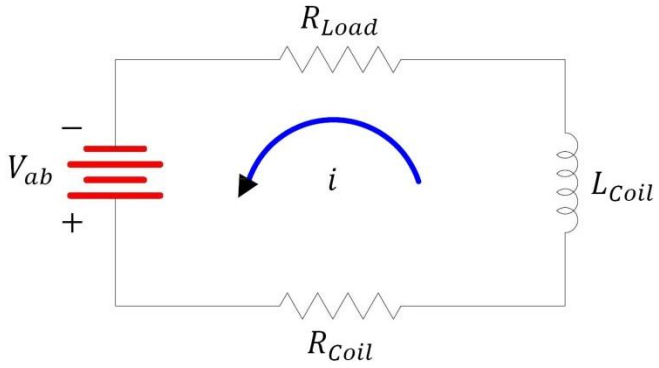

Figure 3-3: Electrical Circuit

$$L_C \frac{di(t)}{dt} + (R_C + R_L) i(t) = V_{ab} \tag{3-17}$$

$$i(t) = \frac{V_{ab}}{(R_C + R_L)} \tag{3-18}$$

One of the important parameter to optimize is the electromagnetic damping (D_{em}) to maximize the power extracted from the harvesting system. Electromagnetic damping can be defined as a function of power dissipated in the coil and the load as shown in (3-19).

$$D_{em} = \frac{V_{ab}^2}{(R_L + R_C) v^2} \tag{3-19}$$

Maximum damping will be produced when the external load is zero. This is when the harvester coils are short circuited and all the energy is dissipated inside the coils. By combining (3-17) and (3-1), a fully developed relationship between output voltage and input forcing function can be determined by converting to frequency domain. When a forcing function is inputted, the closed loop voltage can be determined.

$$\frac{V(s)}{F(s)} = \frac{R_L N B_m \left(r_p^2 - r_m^2\right) \pi s}{\tau_p (R_C + R_L)(ms^2 + (D_{mech} + D_{em})s + k)} \tag{3-20}$$

Some of the dependent variables such as magnet to coil ratio, magnet to iron ratio, load resistance, and coil resistances will be further studied to optimize the system for maximum performance.

3.1.3 Coil Winding and Fill Factor

Coil winding is extremely important parameter for the energy harvesting system. Number of turns per coil determines the resistance of the coil and the load as well as the voltage and power outputs. Within a given area, number of turns in a coil can be determined by (3-21). Where L_w is length of winding wire and D_{Wire} is the diameter of winding wire.

$$turns = \frac{(r_s - r_c)L_w}{D_{Wire}^2} \tag{3-21}$$

Total fill factor should be maximized for maximum number of turns. Fill factor is the amount of area covered by copper wire within a given space. Fill factor for one coil can be determined by (3-22).

$$fillfactor = \frac{turns(\pi r_{wire}^2)}{(r_s - r_c)L_w} \tag{3-22}$$

The fill factor obtained is 0.79 for a circular magnet wire. The number of turns wound in a coil should be maximized as much as possible if the application requires high voltage. For applications required larger voltage, thinner copper wire should be used to increase the number of turns wound. On the other hand, applications requiring higher current must reduce the number of turns by decreasing the wire gauge size.

3.2 Design

Electromagnetic harvesters available are either designed for rotational or linear applications. Electromagnetic voltage and power generation depends on the size and the design. Rotational generators are not as popular in harvesting vibrational kinetic energy as it requires rotating mechanism to work. On the other hand linear electromagnetic energy harvesters can readily harvest vibrational kinetic energy and can be miniaturized for macro and micro scaled applications.

Linear energy harvesting system can be either tubular or planar configuration as depicted in Figure 3-4. Benefit of tubular energy harvester is that the force density is higher than the planar machine so the damping in the system tends to be higher when the velocity is constant. Both the tubular and planar type of energy harvesters has to consist of magnet and

a coil at minimal configuration. Magnet moves relative to the coil or the coil can move relative to the magnet. Type of configuration is dependent on the harvester design. Design where magnet moves relative to the coil has more benefits as the magnets would produce higher inertial velocity due to greater mass of the magnet as compared to the coil. Complete flux reversal across the coil can also be achieved when the magnet moves relative to the coil which translates into higher voltage produced [20].

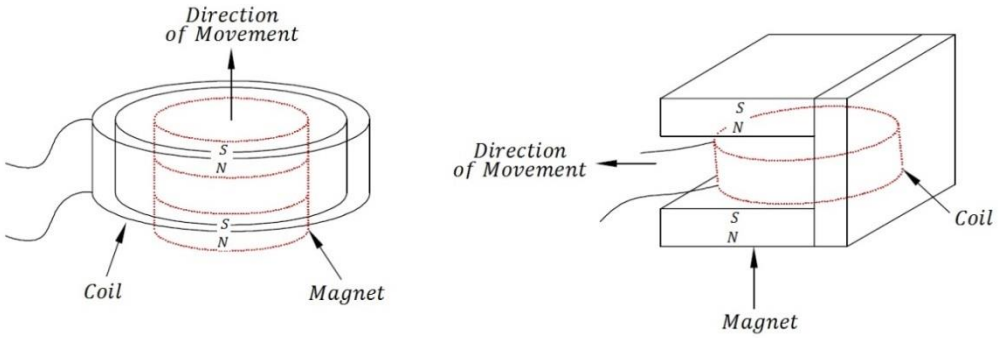

Figure 3-4: Tubular and Planar Harvester

For optimization of electromagnetic energy harvester many design aspects have to be considered. Type of magnet, coil, magnet to coil ratio and the arrangement of magnets is very important. Amount of voltage and power produced is highly dependent on the type of magnet chosen. There are various available permanent magnets to choose from. Strongest available permanent magnet is Neodymium Iron Boron (NdFeB) and its properties are listed in Table 3-1 along with other types of permanent magnets.

Type of Magnet	B_r(T)	$(BH)_{max}$ (KJ/m^3)
Alnico	0.8-1.09	31-42
Samarium Cobalt	0.9-1.1	160-225
Neodymium Iron Boron	1.0-1.35	280-413.8

Table 3-1: Rare earth permanent magnets [21]

NdFeB magnets have a strong magnetic field which is referred to as remnant flux density (B_r). Available energy under the BH curve is also significantly higher for NdFeB; however they can only be used for applications that produce low heating. NdFeB demagnetization

temperature (Curie temperature) is around (80-180 ^{o}C) as compared to alnico magnets (400-450 ^{o}C). Alnico and samarium cobalt magnets suffer from low remnant flux density as shown in Table 3-1 which is not ideal for energy harvesting purposes. For the current AA size harvester the NdFeB magnets were chosen due to its benefits and the working temperature of the entire harvester will not reach a point where the permanent magnet wound become demagnetized.

Special magnet arrangement configurations have been looked at to maximize the magnetic field strength in the air gap. Firstly, one large axial magnet in Figure 3-5 has been used to determine the air gap flux density. Air gap flux density is plotted and it is determined that the air gap flux density is approximately zero in the middle while the top and bottom of the harvester has maximum flux density. Only the top and bottom coils would be excited while the middle coils would produce zero voltage. Several other assemblies shown in Table 3-2 have been studied. Iron poles have been used in between radial and axial magnets to guide the magnetic field and reduce flux leakages.

Magnetic Configuration	Maximum Flux in Air Gap (T)
Axial (up)	0.35 (ends)
Axial and radial	0.445
Radial (inward and outward)	0.16
Axial with iron pole	0.38

Table 3-2: Flux density of various magnetic configurations

The best configuration consists of axial and radial magnets, however radial magnets are very difficult and costly to manufacture so the next best option of axial magnet with iron pole is chosen for the energy harvesting system. With the axial magnet and iron pole configuration. The magnetic field loops through all the coils shown in Figure 3-8 which means that the voltage produce would be higher than just axial magnets. Further optimization approaches will be carried out to optimize the axial magnet to iron pole ratios for maximum magnetic flux in the air gap and will be covered in section 3.3. Also it is important to note that the configurations shown from Figure 3-6 to Figure 3-8 have been studied before in [22] for an

electromagnetic damper and the results are validated here as the energy harvester is of micro size.

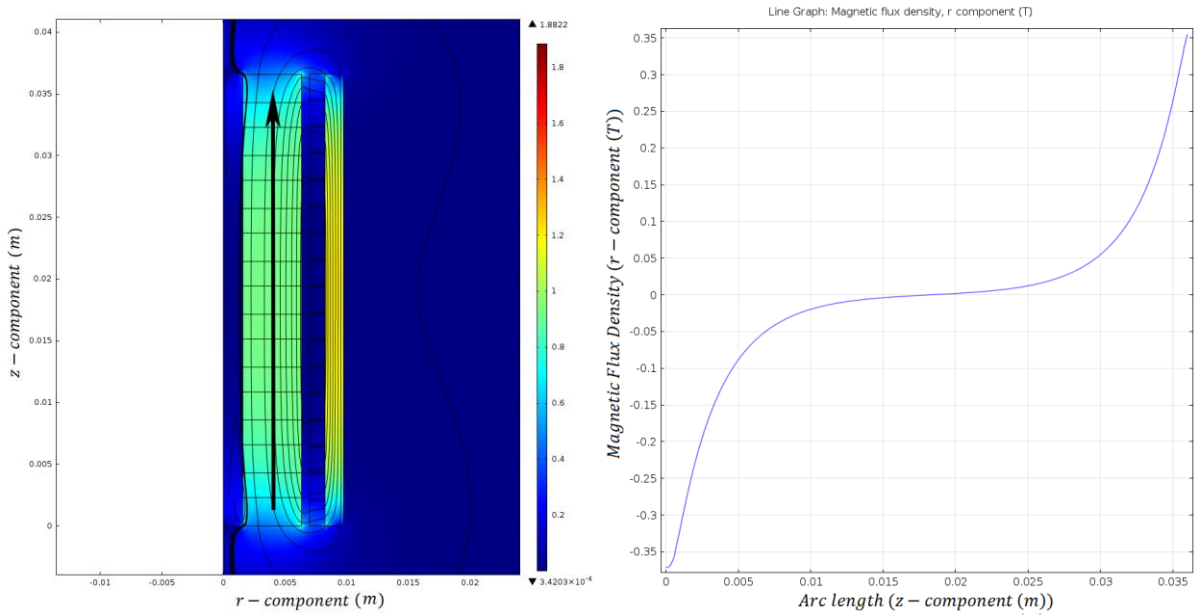

Figure 3-5: Magnetic field formed by one axial magnet (left) and flux density in the air gap (right)

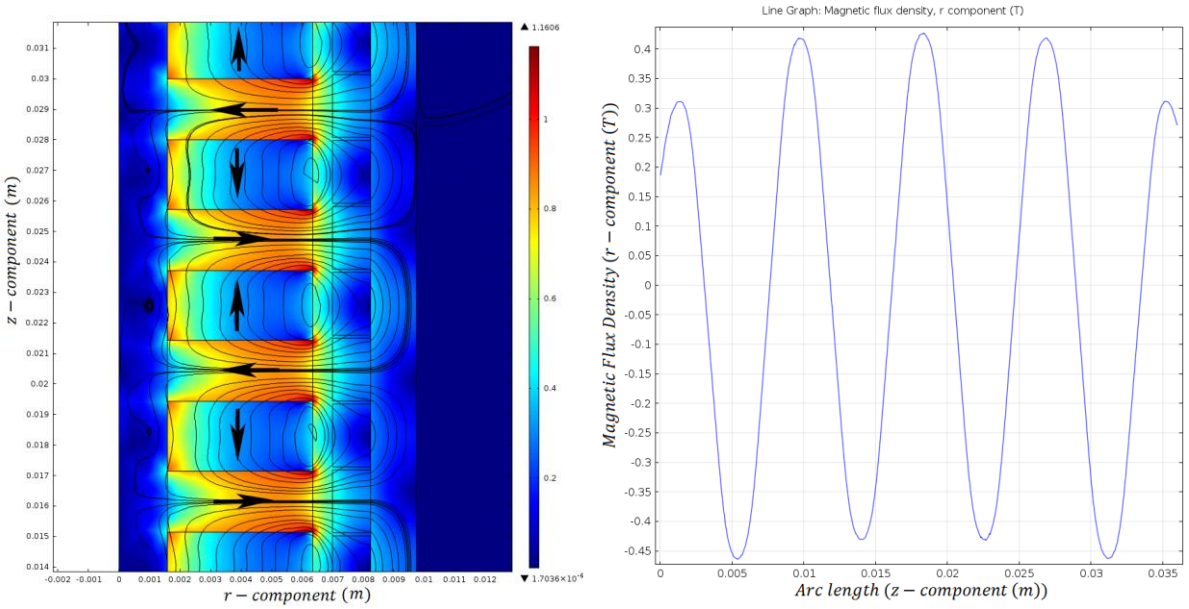

Figure 3-6: Axial and radial magnet configuration (left) and air gap flux density (right)

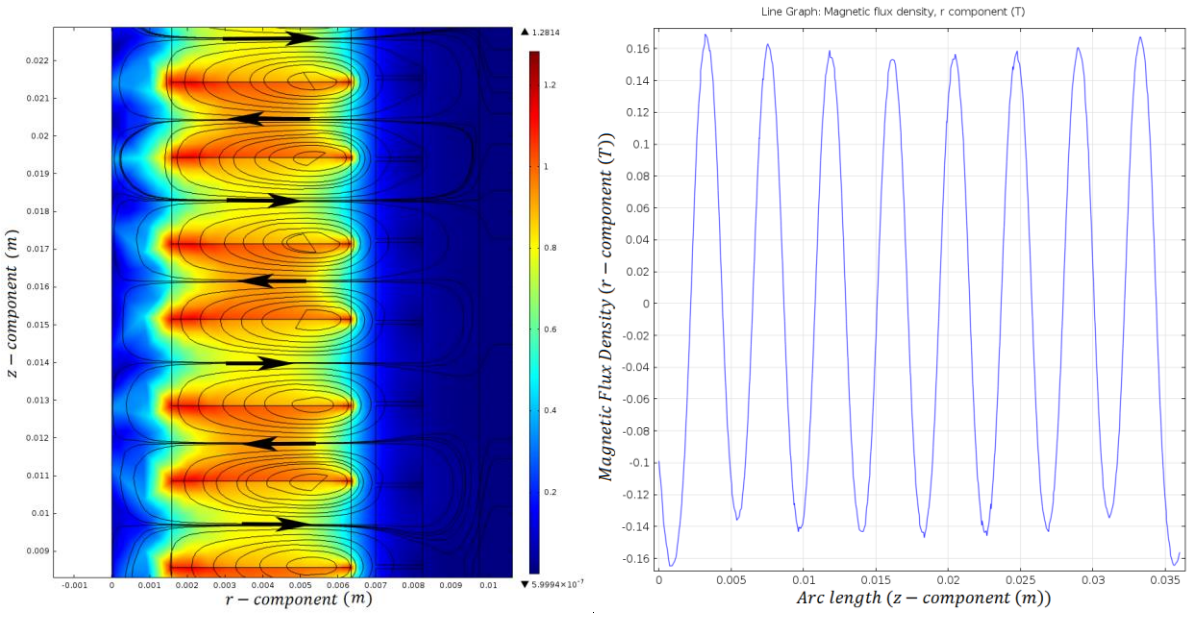

Figure 3-7: Radial magnet configuration (left) and air gap flux density (right)

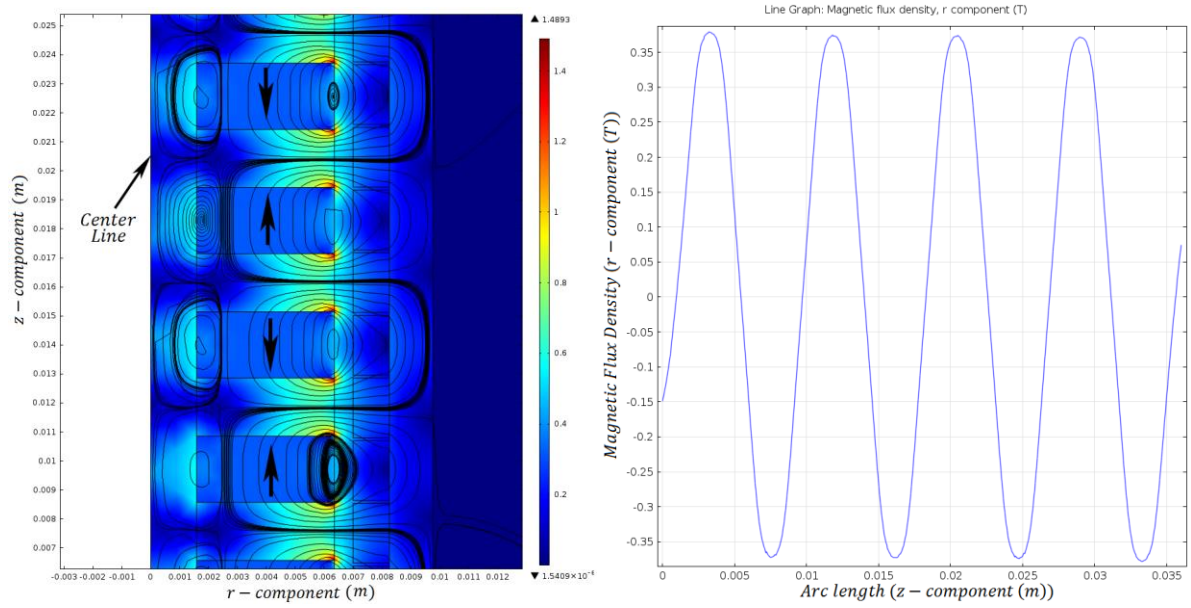

Figure 3-8: Axial magnets and iron pole configuration (left) and air gap flux density (right)

3.3 Prototyping and Testing

3.3.1 Testing Procedure

The testing of the harvester was done using the Modal Shop 2075E shaker, LMS Scadas DAQ, PC and accelerometer to determine the acceleration of the shaker at different frequencies. The fixture is shown below in Figure 3-9.

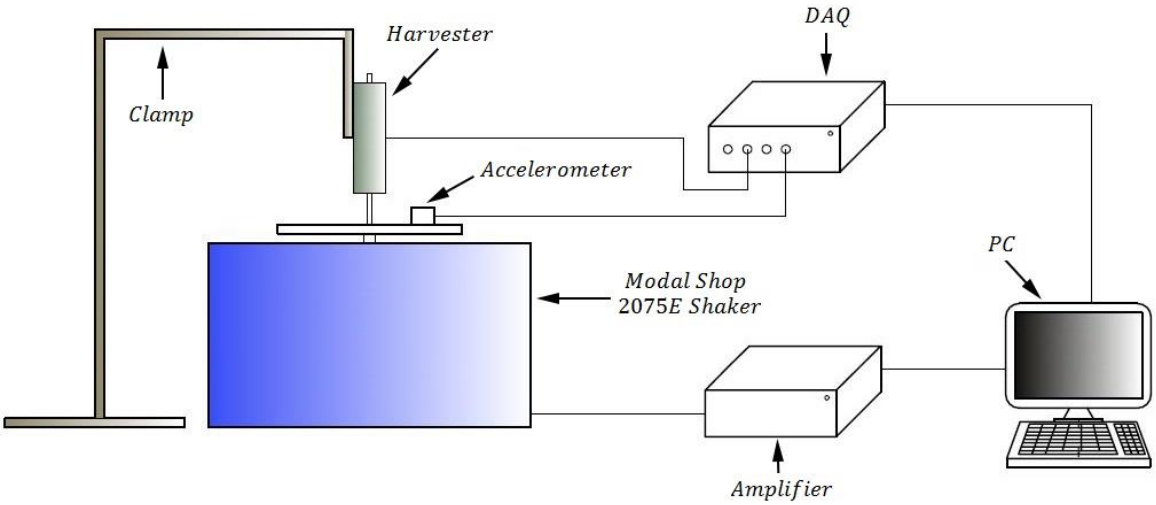

Figure 3-9: Harvester testing fixture

Mover was clamped onto the shaker while the stator was mounted on a clamp. Outputs were connected to the data acquisition system. Accelerometer was mounted onto the shaker plate to determine the acceleration levels and to provide feedback to the system. Accelerometer was connected to the DAQ and the DAQ was connected to a PC for controlling, gathering and storing voltage, acceleration and displacement data. Shaker was given sinusoidal inputs at constant displacements of 1.8 mm to 7.2 mm at frequencies of 5-35 Hz. Peak and RMS outputs of coil voltage, mover acceleration and velocity were gathered. It is important to note that the Modal shop shaker was not designed to operate at very low frequencies of 1-4.5 Hz. Figure 3-10 shows the payload curve of the shaker and it can be seen that the shaker only works for frequencies that are higher than 4.5 Hz. Shakers operation range is limited to its payload curve so it is very important to find a suitable range where displacement will be constant at all frequencies.

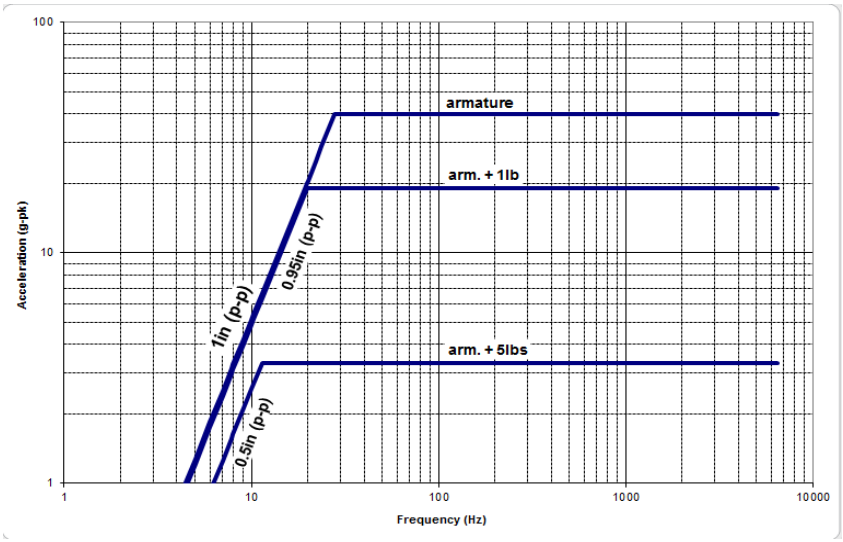

Figure 3-10: Payload curve for Modal shop 2075E shaker [15]

3.3.2 Linear Energy Harvesting System

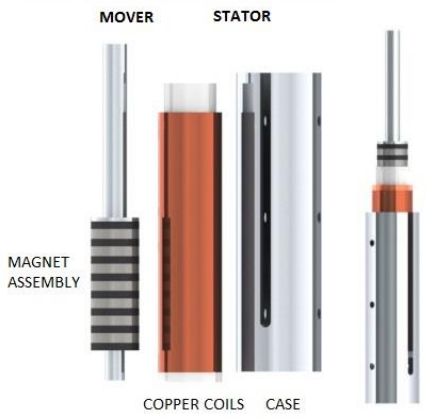

Figure 3-11: Linear energy harvesting system [20]

Goal of linear energy harvesting system is to develop AA size battery harvester that can potentially replace batteries. Prototyped AA size harvester comprises of a mover and a stator. Mover has a magnetic assembly which consists of permanent magnets, cylindrical rod and iron pole while the stator consist of an outer case, copper coils and delrin holder for the coils. Schematic in Figure 3-11 shows the complete assembly of the AA harvester. Linear harvester was designed based on the permanent magnet to iron pole ratio τ_m/τ_p of 1.25 and permanent magnet to coil ratio r_p/r_s 0.73 as described in [22]. Wire gauge of copper wire is chosen to

be 31 and the number of turns wound per coil is 18. Parameters of the harvesters are shown in Table 3-3.

Parameter	Value	Unit	Parameter	Value	Unit
τ_p	1.6	mm	r_t	8.6	mm
τ_m	2	mm	l_m	30	mm
r_m	2.5	mm	l_s	36.8	mm
r_p	5	mm	# of Coils	22	
r_c	5.65	mm	Number of Turns	18	
r_s	6.85	mm	AWG	31	

Table 3-3: Parameters for Prototype I

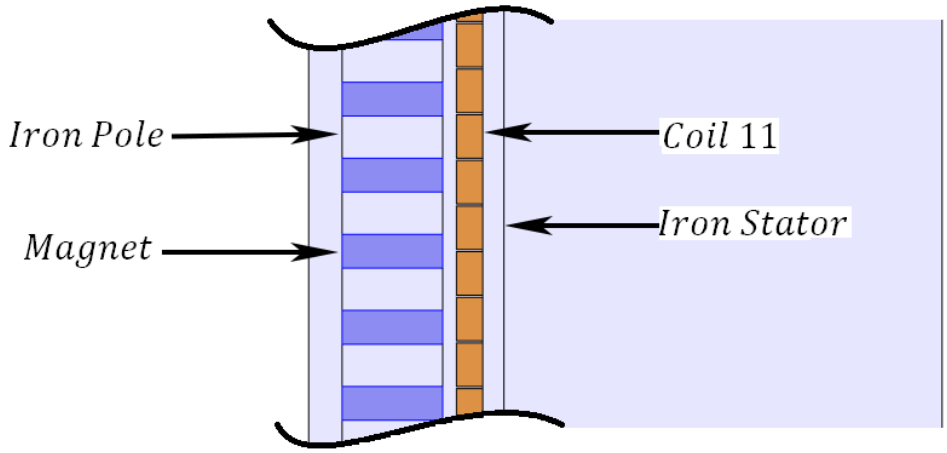

Figure 3-12: Location of coil 11

Developed linear harvester was tested with the equipment shown in Figure 3-9 at 15 Hz with displacement of 1.8 mm to 7.2 mm. First test was conducted on coil 11 to find voltage of a single coil to validate the analytical solution and to determine the best configuration for connecting rest of the coils. Location of coil 11 is depicted in Figure 3-12 for visual understanding.

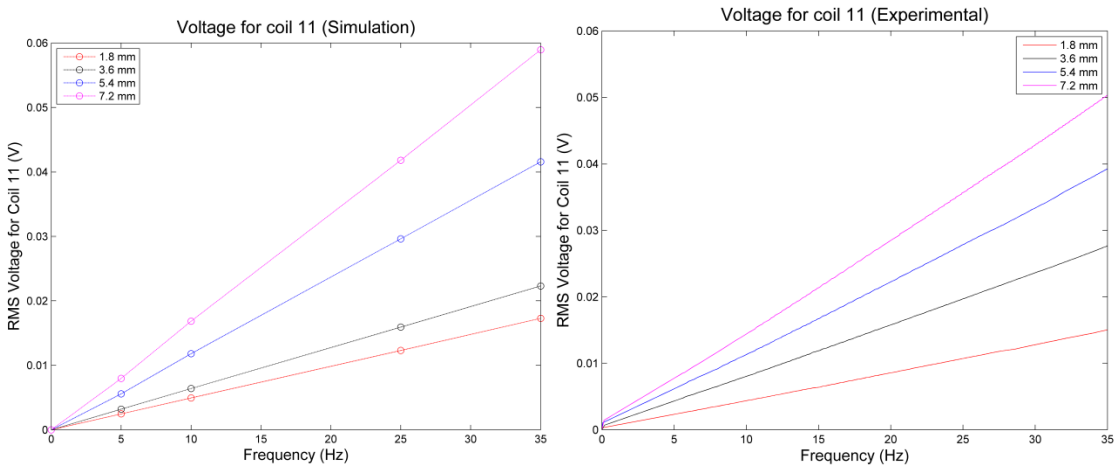

Figure 3-13: Simulated (left) and experimental (right) voltage generation of coil 11

Simulation and testing is done at constant displacement from frequencies of 5-35 Hz and the trend is predicted for experimental results for 0-5 Hz as the shaker was not capable of operating at frequencies of 0-5 Hz. Open loop voltage is shown in Figure 3-13 for both simulated and experimental results. At constant displacement of 7.2 mm, the maximum voltage produced by coil 11 experimentally is 0.0504 V and 0.058 V by simulation. One of the reasons for voltage difference is inaccurate manufacturing of coils. Coils were wound by hand so the number of turns per coil varied from 17-20 turns. There were also assumptions made in the simulation such as magnetic field in the magnet and the stator is purely axial while the magnetic field in the air gap and iron pole is purely radial. This can be seen in Figure 3-8 where the black lines represent the flux density. From simulation it is also determined that the magnet/ Iron pole stack forms closed loop circuit which gives rise to phases in different coils. By studying just one stack as shown in Figure 3-2, it is determined that coil 1 will produce voltage in opposite direction to coil 3, while coil 2 will produce very little voltage from leakage of flux within the magnet/ Iron pole stack. It is very important to connect coils in a way that they don't cancel each other. The best configuration of connecting all the coils is to connect in Y or Delta formation as there are 3 different phases present. However, as the coils were manufactured by hand, the thickness as well as number of turns varied within each of the coil so it was very difficult to determine all the phases properly. For

this very reason, all the coils were connected in second best configuration of series rather than the optimal Y or delta formation.

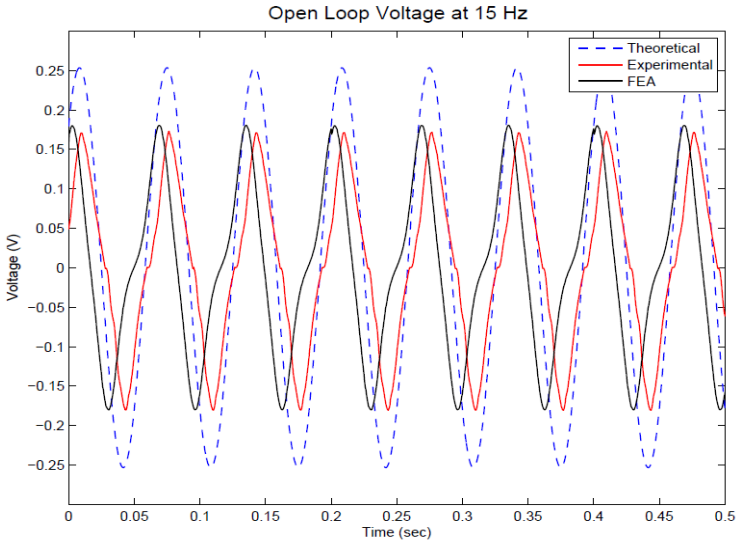

Figure 3-14: Theoretical and experimental open loop voltage induced in the coils at 15 Hz and displacement of 1.8 mm [20]

Test was conducted to compare theoretical and experimental results when the coils were connected in series. There is a good agreement between the FEA and experimental results as seen in Figure 3-14, with approximate error of 3% with a lag. The lag is because of serial connection even though all the coils have different phases. However, the error in theoretical and experimental result is approximately 28% since the phases are not connected appropriately in series.

Power generated from the harvester can be captured only when the coils are connected with external load in series to make the circuit closed loop. As power is a function of voltage and resistance, there must also be load resistance where the power output can be maximized in closed loop circuit [20]. In accordance with power transfer theorem, for maximum power output the load resistance must match the coil resistance. This is investigated by conducting experiments by changing load resistance from 0-32 Ω as shown in Figure 3-15. Total coil resistance was measured to be 6.2 Ω. From Figure 3-15 it can be seen that the power output is maximized at 6.0 Ω. Load matching was done with sinusoidal input to the shaker at frequency of 8 Hz at displacements of 1.8 mm-7.2 mm.

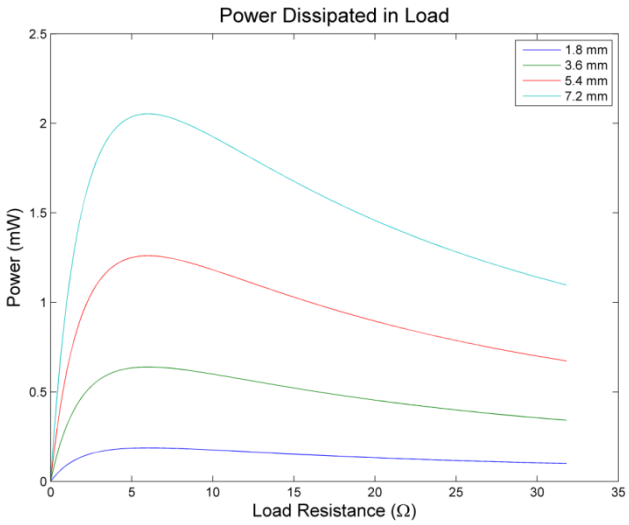

Figure 3-15: Power dissipated in load ranging from 0-32 Ω at 8 Hz and at various displacements ranging from 1.8-7.2 mm [20]

Next set of test conducted were to find the maximum power output of the energy harvester at various frequencies and displacement in closed loop condition when the load resistance was equal to the coil resistance. RMS voltage produced is depicted in Figure 3-16. It can be observed that there is a linear relationship between frequency and the voltage produced. Velocity versus frequency curve is also plotted in Figure 3-17 to understand the linear relationship between voltage and frequency. The velocity of the mover is determined by integrating the accelerometer values. The relationship between the frequency, velocity and displacement is defined in (3-23).

$$V = 2\pi f \cdot A \cdot \cos(2\pi f \cdot t) \tag{3-23}$$

It should be observed in Figure 3-17 that the relationship between velocity and frequency is linear. Displacement also has an effect on the velocity as higher displacement tends to increase the velocity. It is critical to increase the displacement as well as frequency as they also affect the EMF produced according to Faraday's law in (3-14). The RMS voltage in Figure 3-16 is predicted at frequencies lower than 5 Hz while from 5-35 Hz as there are limitations on the shaker.

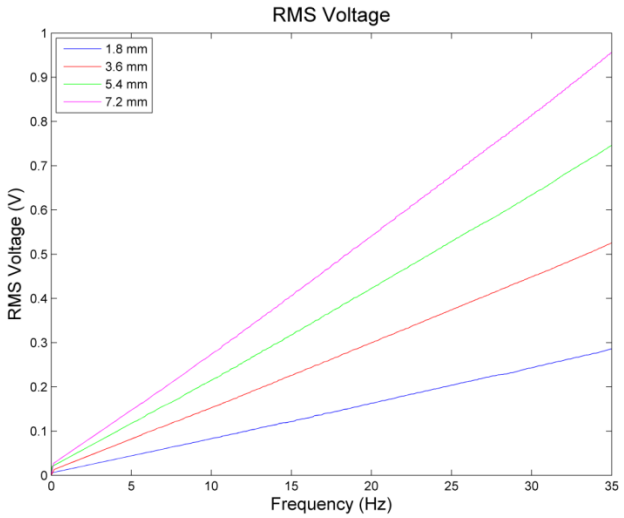

Figure 3-16: RMS Voltage produced at various peak to peak displacements [20]

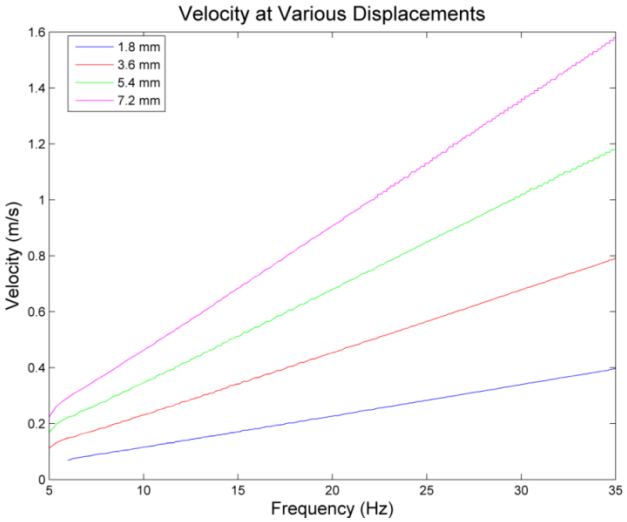

Figure 3-17: Velocity at various frequencies and displacements [20]

The total power dissipated in load is determined in Figure 3-18 when the load is matched with coil resistance. Maximum power dissipated in load is predicted to be 0.9 mW at 7.2 mm displacement at frequencies of 0-5 Hz while the harvester is capable of harvesting 3.1 mW of power at 10 Hz when the displacement is 7.2 mm displacement as shown in Figure 3-18. The power dissipated in load is proportional to the square of the frequency so the highest power dissipated in load is at 35 Hz at 38 mW [20]. The flaw with linear harvester was that the magnet length l_m was of half the length of the coils l_s so for any given amplitude, only half

of the coils were excited. When coils were connected in series, the power dissipated was low as the dead coils also contributed to increase the total resistance of the system. FEA simulations will be conducted in next section to determine if the τ_p/τ_i and r_p/r_s ratios used in linear harvester to produce optimized results for a given volume of energy harvester.

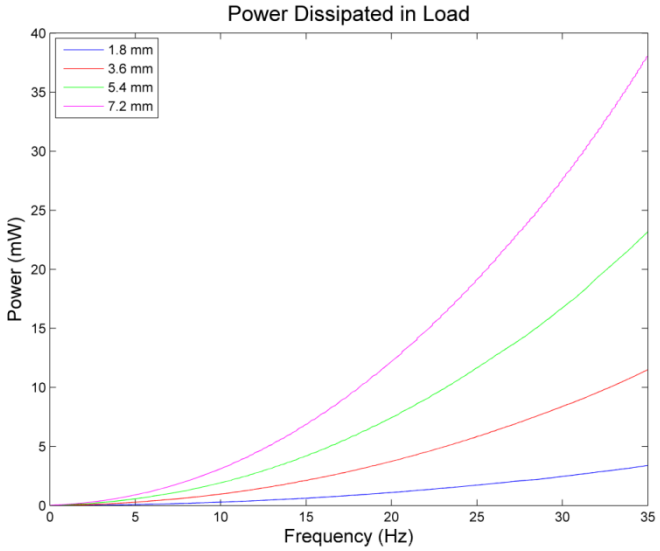

Figure 3-18: Power Dissipated in load at frequencies from 0-35 Hz and at displacements ranging from 1.8-7.2 mm [20]

3.3.3 Simulation

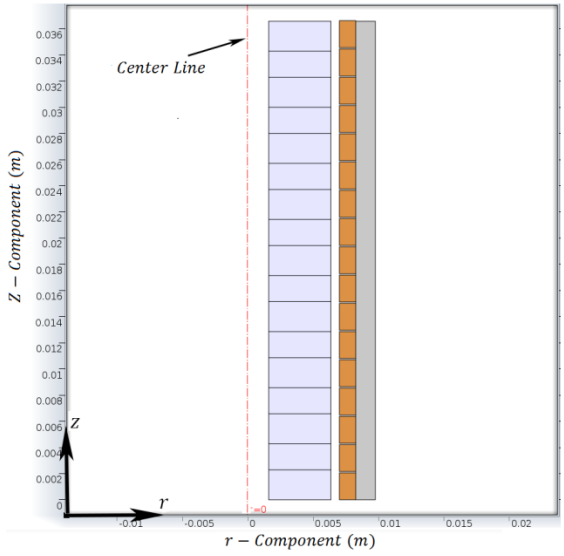

Figure 3-19: Harvester used for optimization

Simulation for the optimization of energy harvester was carried out in comsol to determine the correct ratios. Based on the volume constraint the energy harvester length was chosen at 37 mm and the diameter of 19 mm. Geometry shown in Figure 3-19 was used to optimize. As the energy harvester had a volume constraint, some of the variables that could be optimized were the permanent magnet to iron pole ratio τ_m/τ_p and the permanent magnet to coil ratio r_p/r_s. Simulations were carried out with the τ_m/τ_p ratios ranging from 0.3636 to 11 while the r_p/r_s ratios varied from 0.575-0.8563. It is important to keep in mind that the simulation for the optimization was carried out at frequency of 15 Hz and displacement of 1.8mm. Low displacement and frequency was selected to increase the speed, efficiency and accuracy of the simulation. Based on the fill factor of 0.79 number of turns per coil varied from 27-153 depending on coil width when wire gauge of 34 is used. The results can be observed from Figure 3-20 to Figure 3-22.

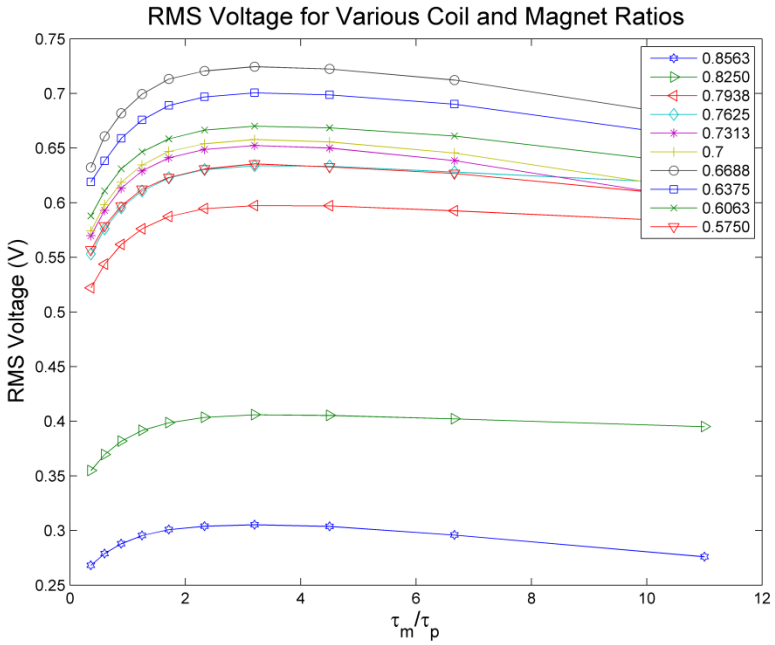

Figure 3-20: RMS voltage when τ_m/τ_p =0.3636-11 for varying r_p/r_s ratios

RMS voltage and power dissipated in coil is maximum when τ_m/τ_p ratio is 3.175 for any given r_p/r_s ratio as shown in Figure 3-20. Also it is important to observe that for τ_m/τ_p ratio

greater than 3.175, the voltage remains relatively constant. However, for ratio lower than 3.175 the voltage drops non-linearly. The smaller optimum τ_m/τ_p ratio of 3.175 is chosen to accommodate low vibrations such that there are three different phases in three coil and that they don't cancel each other out. Maximum voltage generation occurs when r_p/r_s ratio is 0.6688 while the maximum power dissipation in coil occurs when r_p/r_s ratio is 0.7938. The change in ratios is justified by change in number of turns in coil depending on the ratio. With higher number of turns, the voltage is bound to increase but the resistance for coils also increase at the same time. Higher resistance means that the power dissipation in coils will decrease as power is dependent on resistance. For applications that require high voltages, r_p/r_s ratio of 0.6688 should be used but for energy harvesting devices, power dissipated is more important so ratio of 0.7938 will be used.

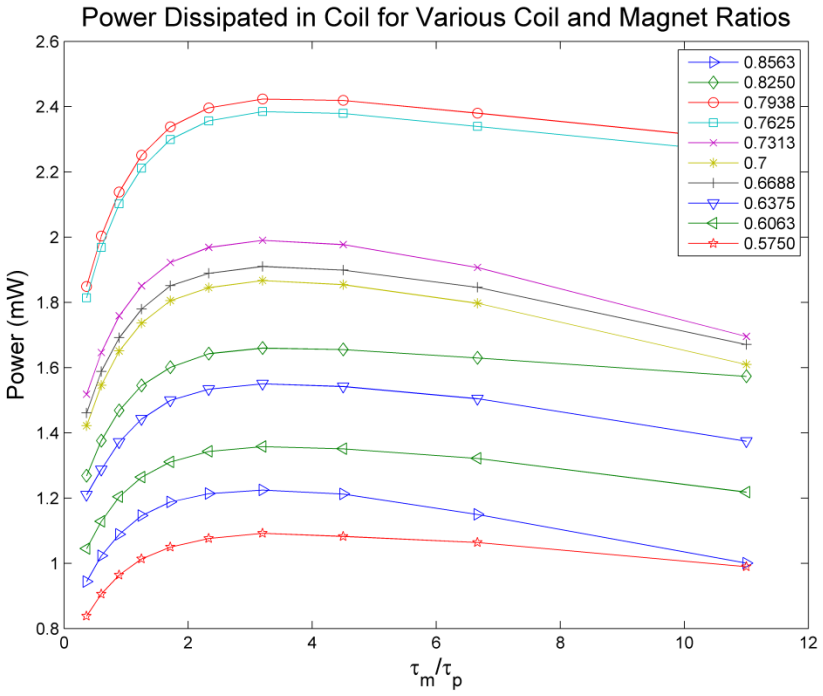

Figure 3-21: Power dissipated in Coil when τ_m/τ_p =0.3636-11 for varying r_p/r_s ratios

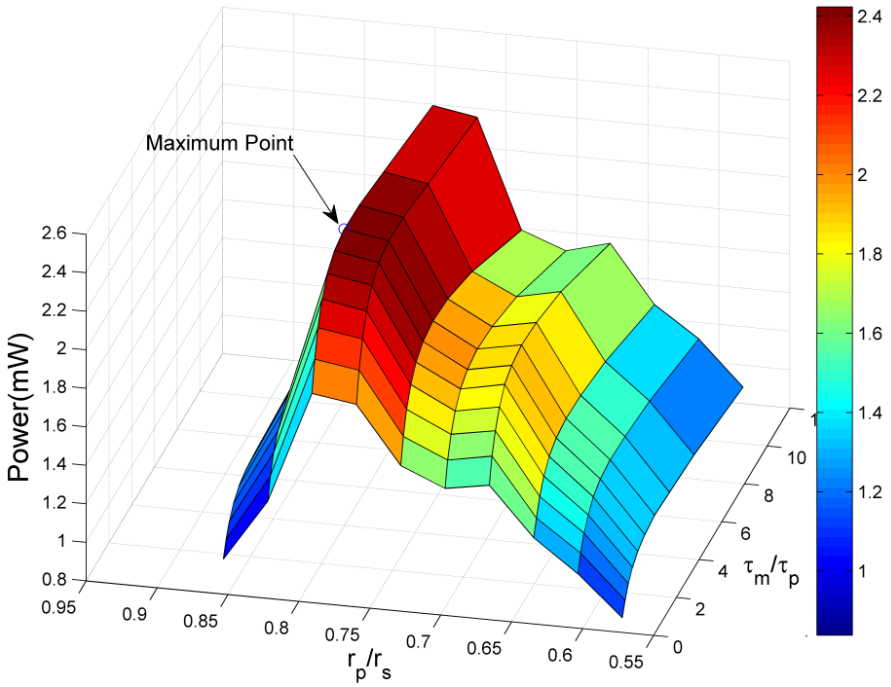

Figure 3-22: Power plot when τ_m/τ_p =0.3636-11 and r_p/r_s =0.5750-0.8563

r_p/r_s and τ_m/τ_p ratios are plotted against the power dissipated. It can be seen from Figure 3-22 that there exists an optimized point for a given volume of harvester where maximum power can be generated. As power dissipation is important for energy harvesting applications, τ_m/τ_p ratio of 3.175 and r_p/r_s ratio of 0.7938 is used.

In chapter 3, a force based linear type energy harvester is developed. This type of harvester does not have a working natural frequency and the power and voltage outputs depend on the velocity. The permanent magnet to iron ratio as well as permanent magnet to coil ratios are optimized. The optimized ratios will be used to develop a non-linear harvesting system covered in Chapter 4.

Chapter 4

Non-Linear Energy Harvesting Device

This section covers the optimization of the linear harvester explained in chapter 3 to build upon a non-linear harvesting system. A new prototype is developed based on the optimization results. Results of an optimized harvester are compared with the linear energy harvesting system. Permanent Magnets are added on the top and bottom of the optimized harvester. Permanent Magnets act as a magnetic spring that can be readily tuned. Section 4.3 expands on the theory developed in Section 3.1 while section 4.4 expands on the design of the non-linear energy harvesting system. Two frequency tuning method are studied and it is found that changing the magnetic air gap of the system is more effective at changing natural frequency as compared to changing the thickness of the stationary permanent magnets. Finally, the device is prototyped and tested to validate the FEA results.

4.1 Optimized Energy Harvesting System

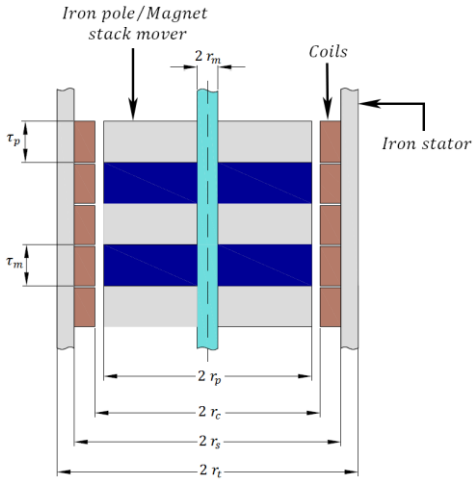

Figure 4-1: Optimized Energy Harvesting System

An optimized energy harvesting system was developed based on the simulations conducted from comsol in section 3.3.3. The optimized energy harvester consists of N52 NdFeB magnetic rings, iron pole, coils, and iron core as shown in Figure 4-1. The parameters used to develop the new harvester are detailed in Table 4-1. Optimized harvester has a mover of

same length as the stator so that all coils are excited. Another important change in the optimized harvester was the use of AWG 34 as compared to AWG 31 to increase the fill factor for higher voltage outputs. The voltage output for linear energy harvesting system was 0.96 V but for many electronics the voltage requirements are higher so the voltage would need to stepped up to either 3.3 V or 5 V for it to be useful. Numbers of turns in the coils are increase by increasing the wire gauge size to eliminate the need to step up the voltage. The optimized harvester has permanent magnet thickness of 3.175 mm as compared to 2 mm thick permanent magnet rings on linear harvester. Also stronger NdFeB N52 was used as compared to NdFeB N42 for linear harvester. Two harvesters are compared in Table 4-2 and it is apparent that the power density, RMS voltage and Power dissipation abilities for the optimized harvester has improved when same sinusoidal input was given.

Parameter	Value	Unit	Parameter	Value	Unit
τ_p	1	mm	r_t	9.5	mm
τ_m	3.175	mm	l_m	36.575	mm
r_m	1.5875	mm	l_s	36.575	mm
r_p	6.35	mm	# of Coils	17	
r_c	7	mm	Number of Turns	40	
r_s	8	mm	AWG	34	

Table 4-1: Parameter selection for optimized harvester

Parameters	Linear Harvester	Optimized Harvester
RMS Voltage	0.96 V	6.4 V
Power Dissipated in Load	38 mW	284 mW
Volume	8.55 cm^3	10.37 cm^3
Power Density	4.44 E-4 W/ cm^3	2.738 E-2 W/ cm^3
Displacement	7.2 mm	7.2 mm

Table 4-2: Linear harvester comparison with optimized harvester

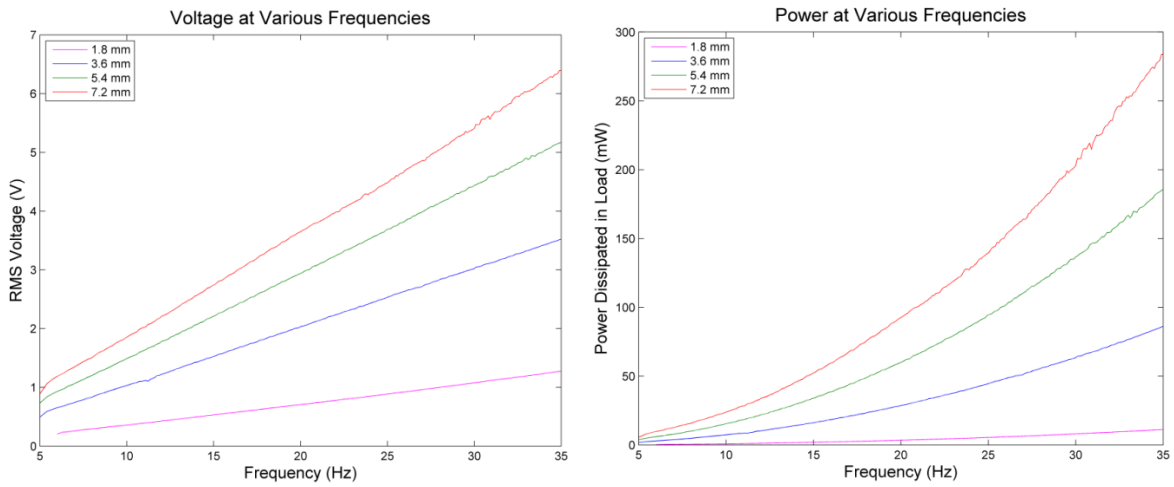

Figure 4-2: RMS Voltage and power dissipated in load for optimized harvester

The testing shows drastic improvement in voltage and power dissipation as observed in Figure 4-2. The maximum RMS voltage output of 6.4 V can be observed at 7.2 mm displacement at 35 Hz while the maximum power dissipation is load is 284 mW. Optimized harvester is of force based type which requires the stator to be stationary while the mover is mounted on a vibrating component. Higher outputs are generated when the mover velocity increases and generally there is no set natural frequency that the harvester will operate at. In daily applications, an inertial type harvester is needed which can resonate at a set natural frequency as many applications have their own vibrating frequency. The next section will comprise of analysis on outdoor power equipment such as snow blower to determine the operating natural frequency. Based on the vibrational testing on snow blower, an inertial type harvester will be developed that used magnetic spring which in this thesis will be called "non-linear harvester" hereafter.

4.2 Snow blower vibrational analysis

Vibrational testing was done on the Craftman 208 cc 24 inch dual stage snow blower to determine the vibrational characteristics [23]. Vibrational measurements were taken at various locations on the snow blower, and the optimal point was identified near the engine as shown in Figure 4-3.

Figure 4-3: Snow blower Vibration Measurement location

Peak acceleration in Figure 4-4 shows that the vibrating of snow blower is up to 2g. To determine the vibrating natural frequency, power spectral density analysis is conducted with the vibrational data gathered as shown in Figure 4-4. Natural frequency of the snow blower is at 21 Hz. Similar vibrational testing is carried out on a lawnmower and power spectral density analysis shows that the natural frequency is 15 Hz.

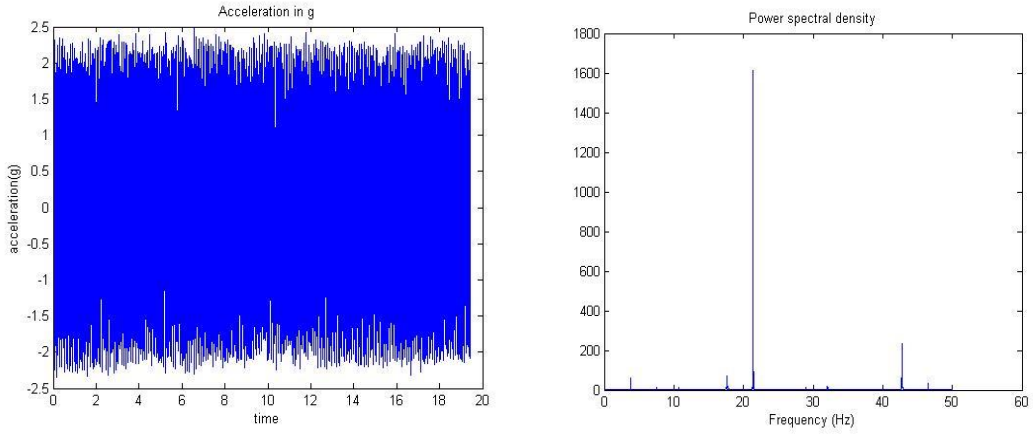

Figure 4-4: Vibrational data with power spectral density

A non-linear energy harvester will be developed to work on lawnmower which uses stationary permanent magnets to act as a magnetic spring. In section 4.3 a detailed theory of the non-linear energy harvester will be developed.

4.3 Theory

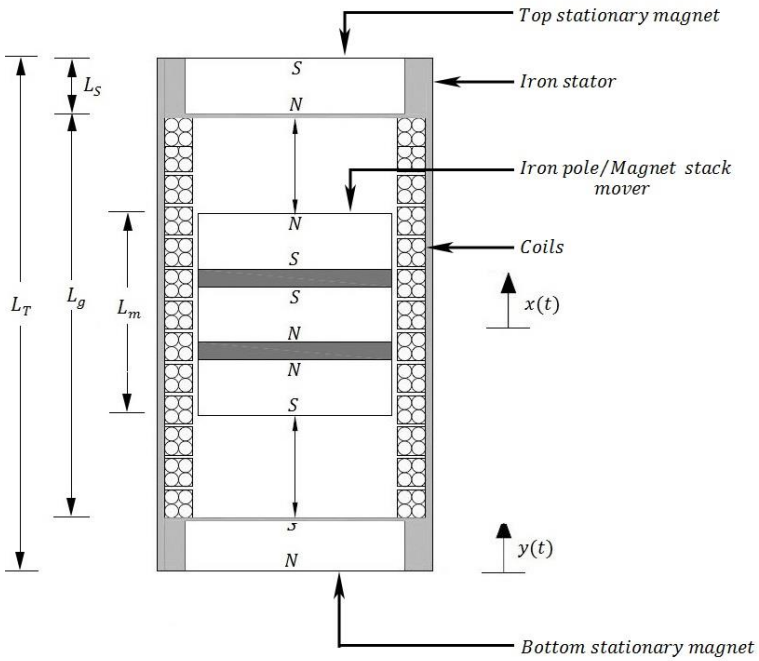

Figure 4-5: Non-linear energy harvester

The optimized energy harvester developed has been used to fabricate the non-linear harvesting system. Non-linear harvesting system uses two oppositely polarized stationary permanent magnets to levitate the middle permanent magnet-iron pole configuration as seen in Figure 4-5. The forces acting on the middle magnet in the vertical direction include the restoring forces created by the oppositely polarized magnets, electromagnetic force created by the coils as the magnet moves up and down and the gravitational force as depicted in Figure 4-6 [5]. The harvester is excited by external vibration where $y(t)$ represents the external displacement and $x(t)$ is the displacement of the inside permanent magnet-iron pole configuration.

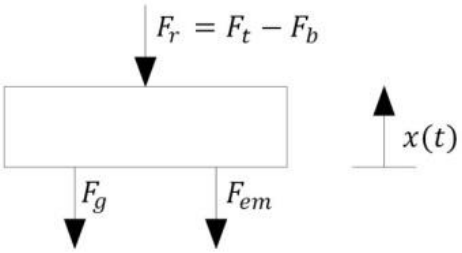

Figure 4-6: Forces acting on the middle magnet-iron pole configuration

Restoring force is determined by FEA simulation in Comsol and by physical testing. Mathematical relationship between the restoring force and central magnet displacement is derived by curve fitting a fifth order polynomial [6]. Resulting fifth order curve derived as:

$$F_r(x) = k_5 x^5 - k_3 x^3 + kx \qquad (4\text{-}1)$$

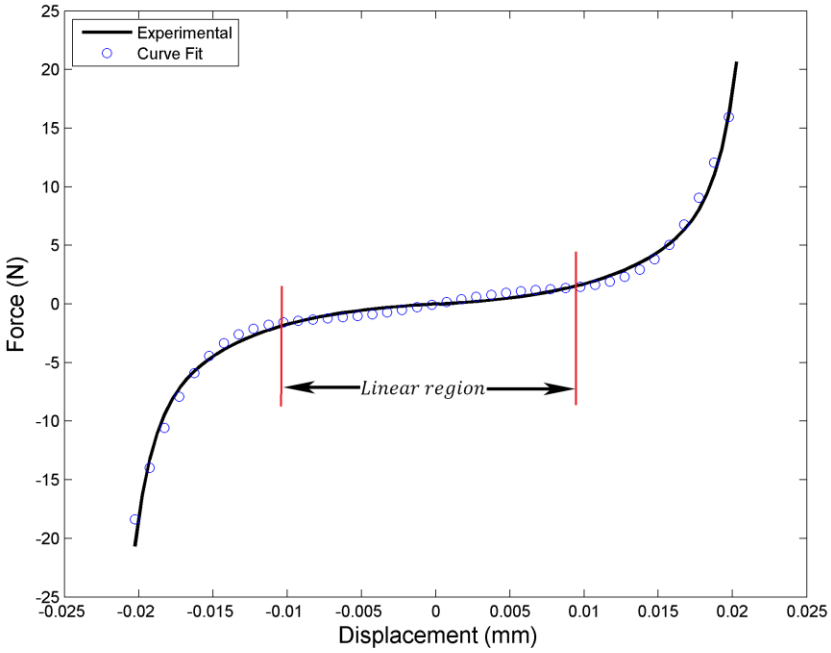

Figure 4-7: Force- Displacement relationship between two repulsive magnets when L_g = 77.1 mm, L_s =9.525 mm

Governing equation of motion for the electromagnetic energy harvesting system in Figure 4-5 can be described as:

$$m\ddot{x} + D_t(\dot{x} - \dot{y}) + k_5(x-y)^5 + k_3(x-y)^3 + k(x-y) = -mg \qquad (4\text{-}2)$$

Where D_t is the total damping ($D_t = D_{mech} + D_{em}$) which is comprised of mechanical damping and electromagnetic damping. k_5, k_3 are non-linear stiffness terms and k is the linear stiffness term. The Electromagnetic damping coefficient is same as the one determined in (3-19) in Section 3.1 as both harvesters consist of similar components. Non-linear and linear stiffness terms are determined from force- displacement relationship between two repulsive permanent magnets in Figure 4-7. It is important to note that the harvester developed works in the linear region as shown in Figure 4-7, but it is also capable of operating in the non-linear region. The harvester developed is called a non-linear harvester because the effect of stationary magnet creates a non-linear spring stiffness within the system. Mechanical damping is determined by inputting a step response into the system (mover) experimentally. Mechanical damping was determined by testing using the fixture shown in Figure 4-8. The harvester is bolted onto the shaker and the accelerometer and the vibrometer are connected to the data acquisition system. System is excited by a step input and the decay in mover motion is captured by the vibrometer.

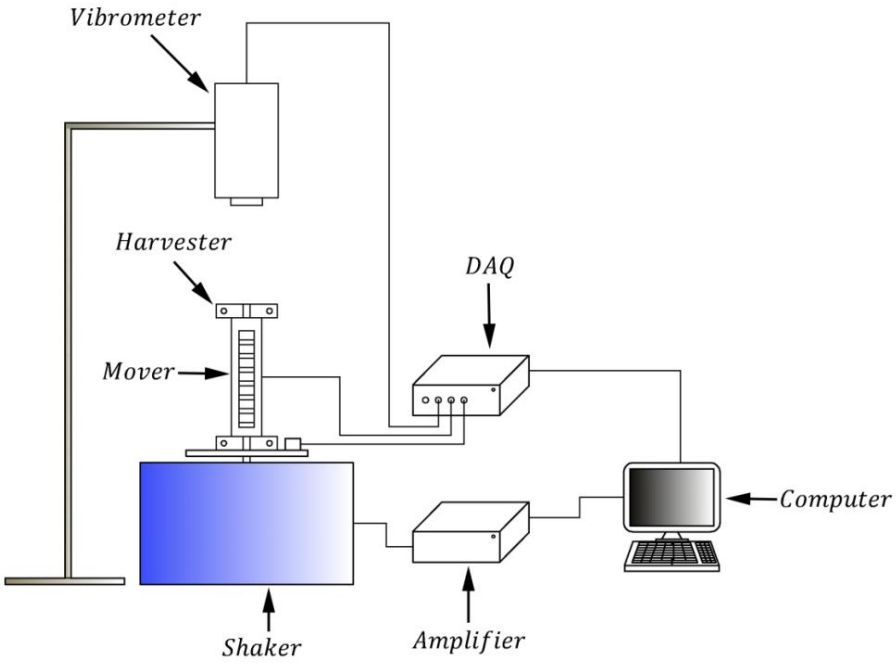

Figure 4-8: Non-linear testing configuration

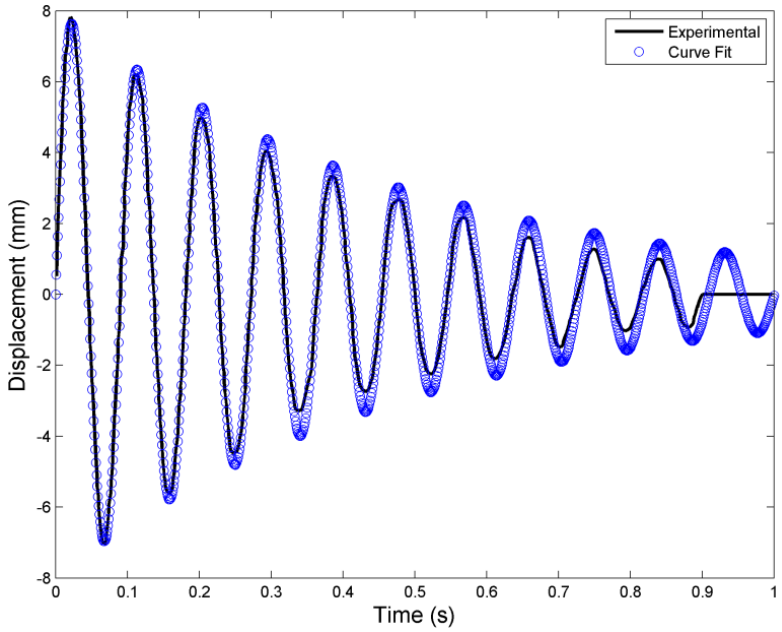

Figure 4-9: Oscillatory response of the mover when L_g = 77.1 mm, L_s =9.525 mm

Oscillations are recorded when the gap is constant at 77.1 mm while the stationary magnet width is changed from 6.35 mm to 12.7 mm. Oscillations are also recorded when the stationary magnet width is constant at 9.525 while the gap is changed from 70.75 mm to 83.45 mm. The oscillation of the system when L_g = 77.1 mm, L_s =9.525 mm are shown in Figure 4-9. Mechanical damping is determined by curve fitting using least square approach method.

$$x(t) = Ae^{-\varsigma\omega_n t}\sin(\omega_d t + \phi) \tag{4-3}$$

Mechanical damping of the system can be found from least square approach by evaluating the decaying term $\varsigma\omega_n$ to find ς, where ω_n is the natural frequency of the system defined as:

$$\omega_n = \sqrt{\frac{k}{m_m}} \tag{4-4}$$

k is the linear stiffness term obtained by 5th order curve fitting in Figure 4-7 and m_m is mass of the mover. The mechanical damping of the system then can be evaluated as:

$$D_{mech} = 2\varsigma\sqrt{km} \tag{4-5}$$

The linear, non-linear stiffness terms as well as natural frequency of the system for various permanent magnet and gap configurations are obtained from force- displacement relationship while the mechanical damping is obtained from the least square approach. All the data is tabulated in Table 4-3.

Variables	L_g = 70.75 mm L_s =9.525 mm	L_g = 77.1 mm L_s =6.35 mm	L_g = 77.1 mm L_s =9.525 mm	L_g = 77.1 mm L_s =12.7 mm	L_g = 83.45 mm L_s =9.525 mm
$k_5 (N/m)$	6.601e9	3.002e9	3.768e9	7.855e9	2.238e9
$k_3 (N/m)$	5.584e5	2.915e5	1.248e5	1.581e6	2.152e5
$k (N/m)$	253.07	154.86	175.74	175.74	111.20
$m_m (kg)$	0.03679	0.03679	0.03679	0.03679	0.03679
$f_n (Hz)$	13.2	10.3	11	11	8.75
$\varsigma\omega_n$	3.26	1.63	2.04	2.04	1.36
D_{mech}	0.24	0.12	0.15	0.15	0.1

Table 4-3: Spring stiffness and mechanical damping of the system

From Table 4-3, it can be seen that the mechanical damping obtained by experimental result is same when the gap L_g is held constant at 77.1 mm while changing the stationary magnet thickness L_s from 9.525 to 12.7 mm. The linear stiffness term k is also identical which makes the natural frequency of the system same. This is because the magnets tend to saturate and the stiffness created by the stationary magnets do not change when changing the stationary magnet thickness. It is also important to observe that as the gap L_g increases, the mechanical damping as well as natural frequency and spring stiffness decreases. During vibration, a turning moment is created due to repulsive forces from the stationary magnet on the mover. The turning moment tends in increase the friction within the system as the mover keeps sliding with the coil holder. So as the spring stiffness increases within the system, the turning moment also increases due to the repulsion from the magnet. It is advisable to increase the gap L_g in the system to decrease the mechanical damping of the system but at a cost of decrease in natural frequency of the system.

4.4 Design

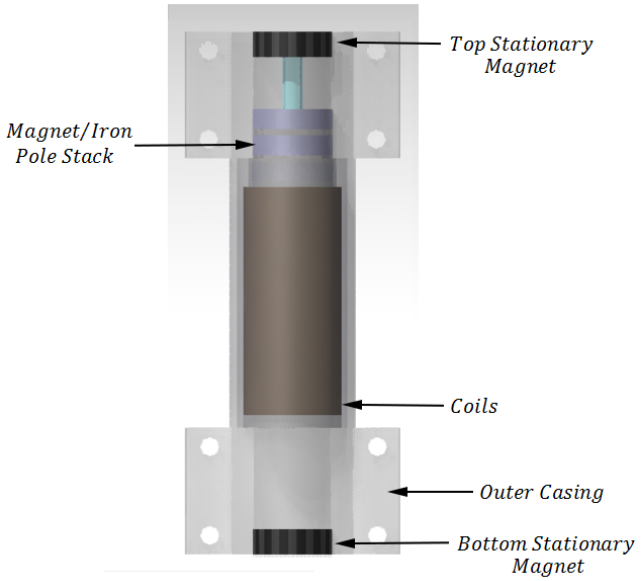

Figure 4-10: Energy Harvester Assembly

The non-linear energy harvesting system consists of two stationary top and bottom magnets, mover consisting of magnet and iron poles while the stator contains the coils, and casing. Complete assembly is shown in Figure 4-10.

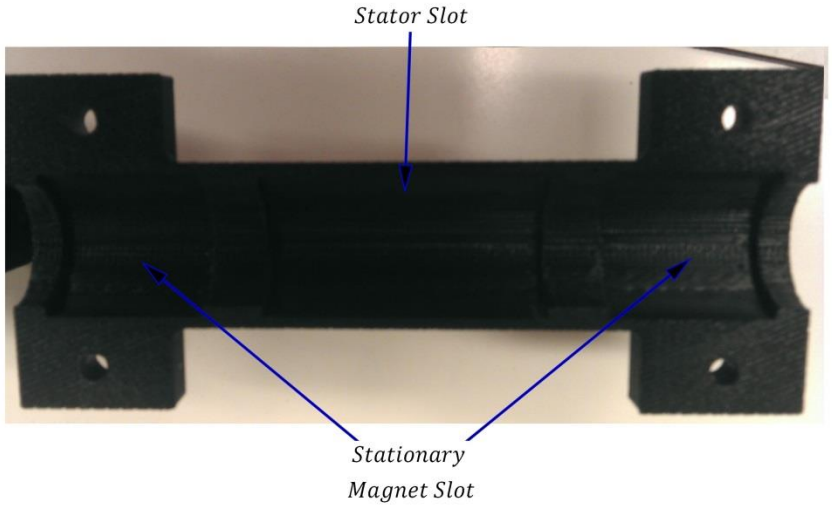

Figure 4-11: Outside casing for non-linear energy harvester

Non-linear harvesting system is made to be robust and could easily be taken apart for repairs or further optimizations. Outside casing is made of ABS from 3D printing. Outside casing is

made into two halves seen in Figure 4-11 and they were later fastened together with bolts and nuts. Casing is also designed such that it can easily be bolted to the shaker plate. Outside casing consists of a stator slot where coil are held in place while the stationary magnet slot holds stationary magnet as shown in Figure 4-11. Ridges on the left and right end of the casing are there to prevent the stationary magnet pieces from moving back and forth when the energy harvester is in operation. Stationary magnets piece contains NdFeB magnets as shown in Figure 4-12. Magnet piece thickness can be increased by adding more magnets or reduced by removing magnets. Magnets are mounted on a 3D printed ABS cylinder.

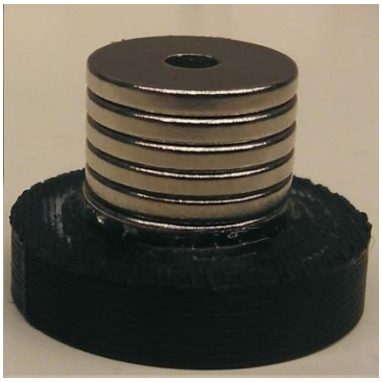

Figure 4-12: Stationary Magnet Piece

Mover consists of a 3.175 mm diameter threaded rod used to hold the magnet and iron poles in place as shown in Figure 4-13. Plastic nuts are used on both sides to fasten magnet and iron poles together so that the magnetic field is diverted through iron poles for optimized harvester performance.

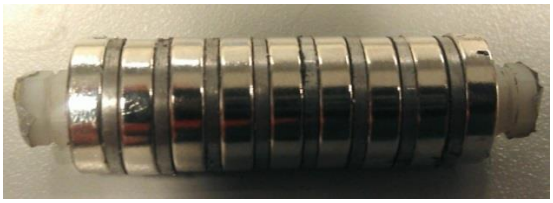

Figure 4-13: Mover consisting of magnet, iron pole, plastic nut and threaded rod

4.5 Simulation

One of the benefits of this non-linear levitation system is that the stiffness of the system can be readily changed by changing the spacing of top and bottom magnet or varying the thickness of the top and bottom magnet. The effect of changing the thickness of the top and

bottom stationary magnet is examined for the harvester using analytical method described in section 4.1. ODE 45 function is used to solve non-linear equations in matlab. Equations in section 4.1 are solved for frequency range of 5-30 Hz with constant sinusoidal acceleration input of $9.8\,m/s^2$ instead of constant displacement. At constant displacement, the acceleration increases exponentially at higher frequencies so it is not a good indicator to determine resonance within the system. Initial parameters such as displacement and velocity are defined to be zero. Variables such as voltage, mover displacement and power dissipation in load are solved with the given parameters shown in Table 4-4**.**

Parameter	Value	Unit	Parameter	Value	Unit
L_m	36.575	mm	D_{mech}	0.1-0.24	
L_g	70.75-83.45	mm	Acceleration	1	g
L_s	6.35-12.7	mm	# of Coils	17	
m_m	0.03679	kg	Number of Turns	40	Turns
R_{Coil}	2.18	Ω/coil	AWG	34	
R_{Load}	37	Ω			

Table 4-4: Parameters used to solve for non-linear harvester

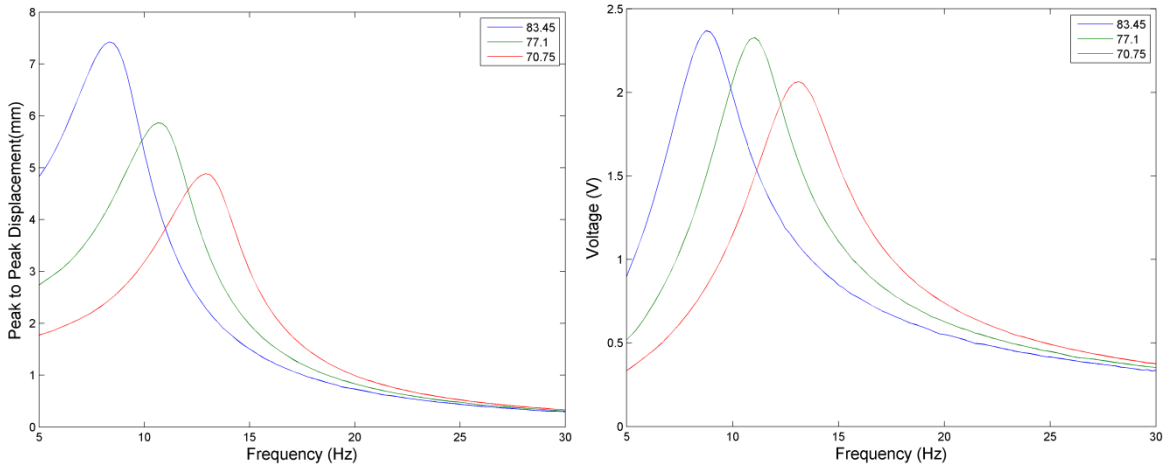

Figure 4-14: Displacement (left) and voltage (right) when L_g = 70.75 to 83.45 for constant L_s

Firstly, the effecting of changing the gap is examined when the magnet thickness L_s is constant 9.525 mm while the gap L_g between the two stationary top and bottom magnets shown in Figure 4-5 is changed from 70.75 mm to 83.45 mm. Effect of changing gap on voltage and displacement is shown in Figure 4-14. As the gap is narrowed the natural frequencies of the system increases while the displacement of the mover decreases. Shift in natural frequency is due to the fact that as the gap decreases, the top and bottom repulsive forces become stronger. Higher Repulsive forces cause the spring stiffness of the system to increases which increases the natural frequency of the system. When the gap is 83.45 mm, the maximum emf generated is 2.33 V while the peak to peak displacement is 7.43 mm**.** When the gap is smallest at 70.75, the emf generated is only 2.04 V while the peak to peak displacement is 4.88 mm.

Another method of changing natural frequency is to change the magnet length (L_s) while keeping the gap (L_g) constant. The magnet thickness is changed from 6.35 mm -12.7 mm while keeping the gap constant at 77.1 mm. The voltage and peak to peak displacement is shown in Figure 4-15. It should be noted that there will come a saturation point where increase in permanent magnet thickness of stationary magnet will not shift the natural frequency. This is the case when the permanent magnet thickness is changed from 9.525 mm to 12.7 mm.

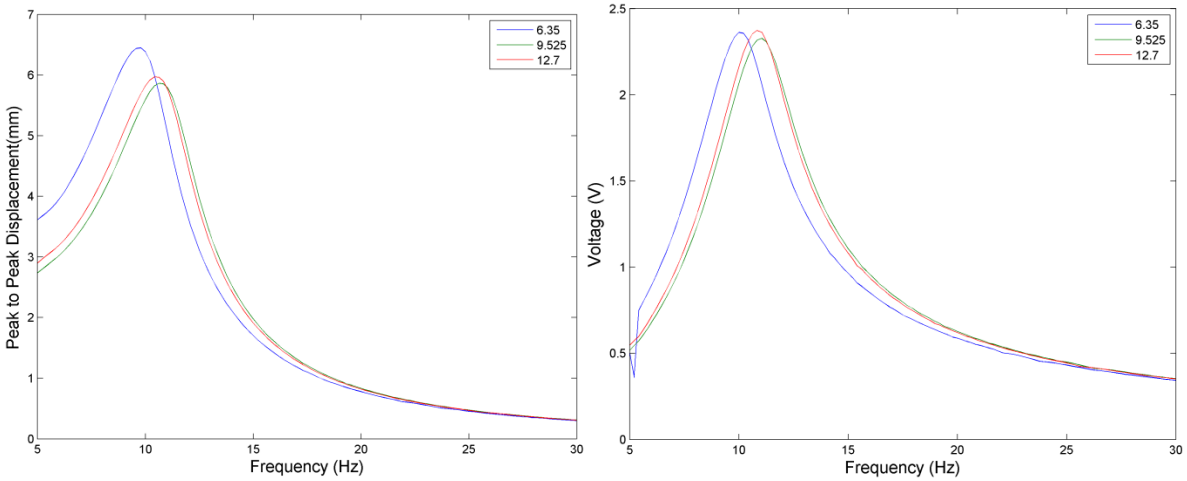

Figure 4-15: displacement (left) and voltage (right) when L_s = 6.35 to 12.7 mm for constant L_g

When magnet thickness is 9.525 mm and the gap is constant at 77.1 mm, the natural frequency of the system is 11 Hz and the emf generated is 2.33 V while the peak to peak displacement is 5.86 mm. Increasing the magnet to 12.7 mm while keeping the gap constant at 77.1 mm shows that the natural frequency is still constant at 11 Hz and the voltage and peak to peak displacement is 2.37V and 5.97 mm.

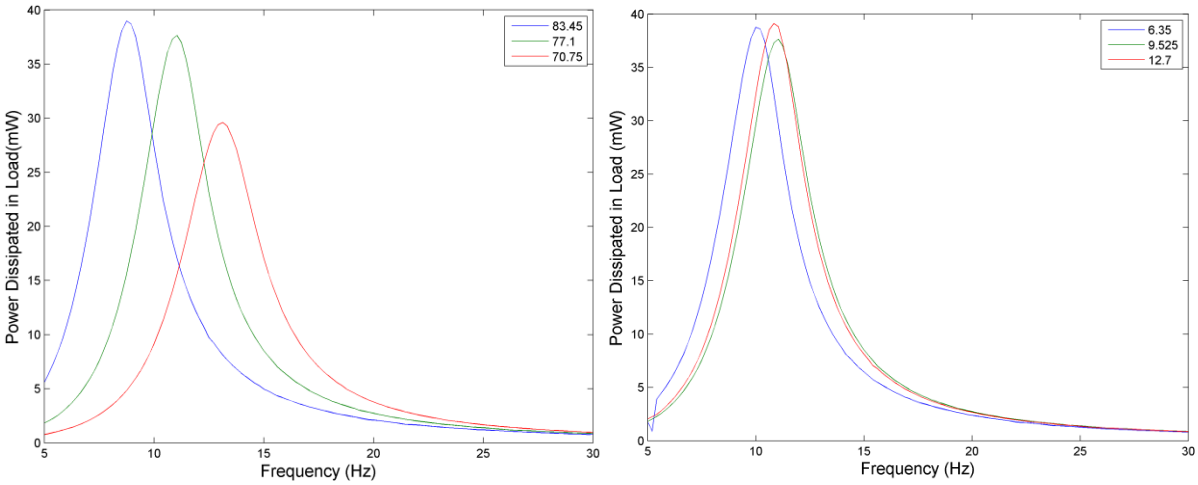

Figure 4-16: Theoretical Power dissipation for change in gap thickness (left) and change in magnet thickness with constant gap (right)

Maximum power dissipated in load is calculated when $R_{Load} = R_{Coil} = 37\Omega$. Power dissipation in load when the gap is changed is shown in the left figure in Figure 4-16 while change in magnet is shown on right. Maximum power dissipation occurs when the gap is 83.45 mm and magnet size of 9.525 mm. Power dissipation in load will decrease if the natural frequency is increased. So it is optimal to lower the natural frequency of the system to achieve highest power dissipation. However, as the non-linear harvester is to be used for snow blower and lawn mower applications, it is optimal to go with gap size of 70.75 mm and magnet thickness of 9.525 mm. The harvester will be tested in the next section and the analytical model will be compared with the experimental model for verification.

4.6 Testing

4.6.1 Force Testing

Repulsive force between the stationary magnet and moving magnet is validated by testing. Force between the moving magnet and stationary magnet is determined with the digital scale and digital height gauge as shown in Figure 4-17.

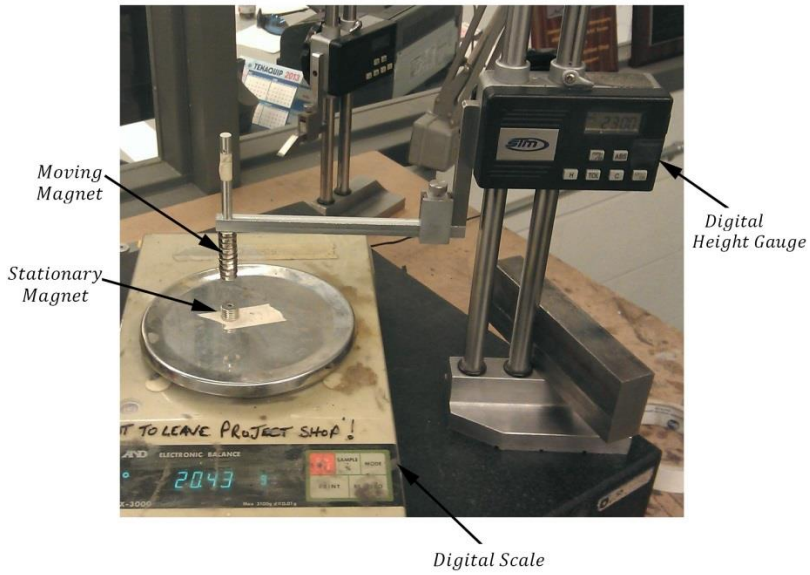

Figure 4-17: Test fixture for force testing

The stationary magnet is fixed on a digital scale while the moving magnet is mounted on digital height gauge. Digital scale is zeroed with the stationary magnet mounted on top. Initially the distance between the moving magnet and stationary magnet is kept to 20 mm. Moving magnet is lowered with increments of 0.25 mm until distance between the stationary magnets and moving magnet is 1 mm. Mass exerted by repulsive magnet on the digital scale is recorded before lowering it further. Repulsive force is found by multiplying the mass by gravity. Force testing is done with stationary magnet of 6.35 mm, 9.525 mm and 12.7 mm thickness. Force versus distance plot can be viewed in Figure 4-18. Repulsive force increases when the stationary magnet thickness in increased. The maximum repulsive force between two magnets occurs when the distance is zero. The FEA results are validated with the experimental results with error less than 2%. In the next section, testing and results of energy harvester are shown and the theoretical model will be validated.

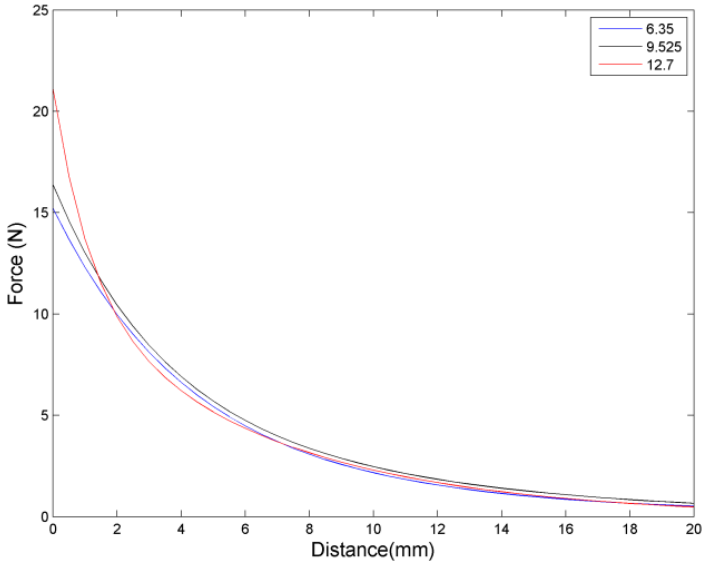

Figure 4-18: Force between stationary and moving magnet

4.6.2 Harvester Testing

Testing of the non-linear energy harvesting system was done on the Modal Shop 2075E shaker, LMS Scadas DAQ, PC, accelerometer and Polytec OFV-505 vibrometer. The test setup is shown in Figure 4-8. Harvester was clamped onto the Modal Shop 2075E shaker. Magnet assembly was free to move as vibrations were induced. The coils and the stationary magnets were clamped tightly with outside casing. Accelerometer on the shaker was used for feedback and to detect the acceleration. Accelerometer was connected to the LMS Scadas DAQ. Laser vibrometer was used to detect the displacement of the mover and it was connected to the DAQ. The DAQ was connected with the computer for data gathering and analysis. Sinusoidal inputs were inputted and the voltage, displacement and acceleration readings were gathered from the test configuration. Several tests were conducted to characterize the non-linear energy harvester. Goal of the non-linear harvester was to readily change the operating frequency of the shaker to match external vibrations. Two ways to change natural frequency of the system is to change stationary magnet (L_s) thickness or change the gap size (L_g).

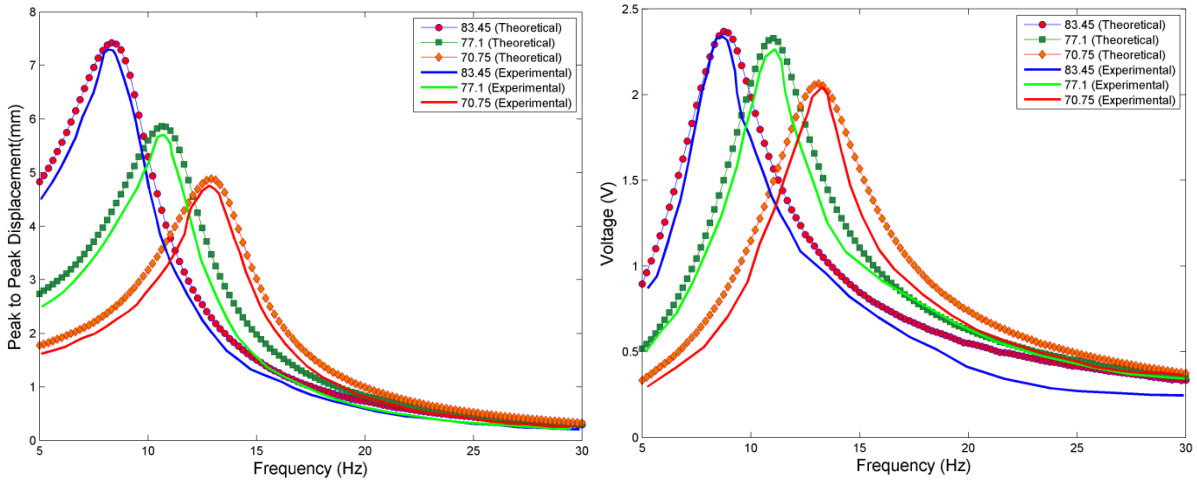

Figure 4-19: Experimental and Theoretical comparison of displacement and voltages when the air gap is changed and the magnet thickness is constant

Gap size was changed from 70.75 mm to 83.45 mm when the stationary magnet thickness was 9.525 mm. Figure 4-19 shows the effect of changing the gap size on natural frequency of the system and is compared with the theoretical model developed in Section 4.3 to validate the theoretical model. Testing was conducted at constant acceleration level of 1g and the tests were done at frequencies of 5-30 Hz using the test configuration in Figure 4-8. Effect of changing the magnet thickness (L_s) on natural frequency was also tested while keeping the gap size (L_g) constant at 77.1 mm and can be seen in Figure 4-20. Experimental results agree well with the theoretical model with some discrepancies. Discrepancies can be due to resolution and operation of testing equipment. The shaker needs to adjust the displacement constantly from the feedback of accelerometer data so the displacements tend to fluctuate with some degree of error. Some of the assumptions in the theoretical model that would lead to discrepancies include no leakage of flux, magnetic field in iron poles and stator is axial while magnetic field in coils in purely radial.

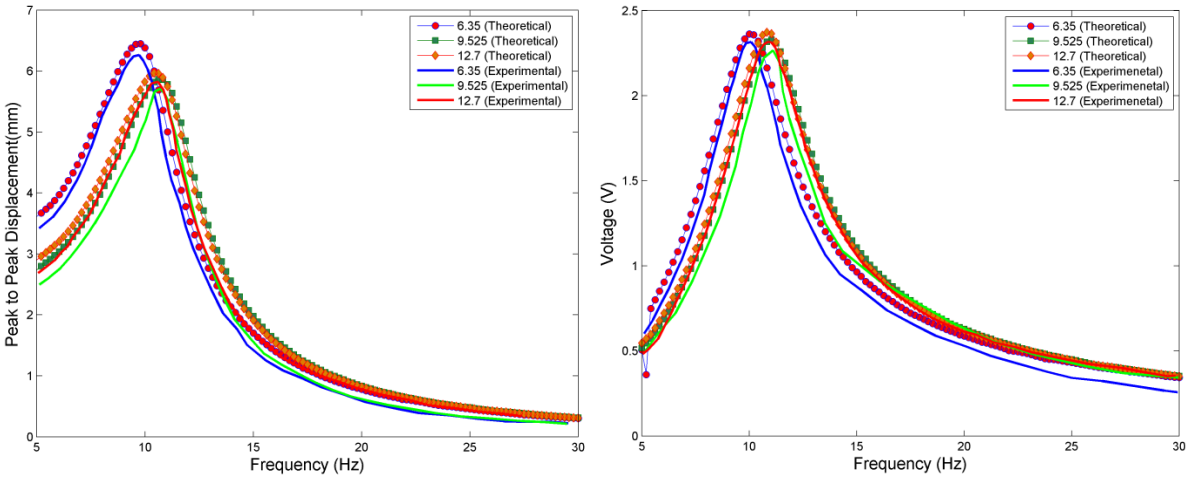

Figure 4-20: Experimental and Theoretical comparison of displacement and voltage when the gap is constant and when the magnet thickness is changed

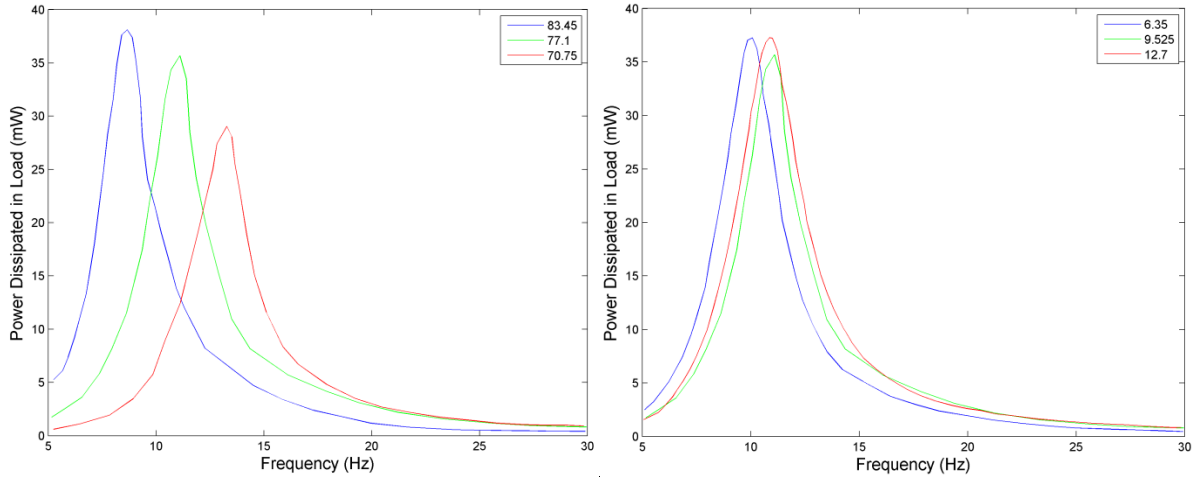

Figure 4-21: Experimental Power dissipation when the gap is changed (Left) and magnet thickness is constant. Change in magnet thickness with constant gap (Right).

Power dissipation capabilities are also tested to determine the amount of power produced which is represented in Figure 4-21. Maximum power generated is 38 mW when L_g = 83.45 mm and L_s = 9.525 mm. Open loop voltage, displacement, power dissipation in load and working natural frequency are summarized in Table 4-5.

Variables	L_g = 70.75 L_s =9.525	L_g = 77.1 L_s =6.35	L_g = 77.1 L_s =9.525	L_g = 77.1 L_s =12.7	L_g = 83.45 L_s =9.525
Simulation (Voltage)	2.07 V	2.36 V	2.33 V	2.37 V	2.37 V
Experimental (Voltage)	2.04 V	2.32 V	2.27 V	2.32 V	2.33 V
Simulation (Displacement)	4.88 mm	6.44 mm	5.86 mm	5.97 mm	7.43 mm
Experimental (Displacement)	4.76 mm	6.26 mm	5.71mm	5.82 mm	7.29 mm
Simulation (Power)	29.62	38.76	37.65	39.13	39
Experimental (Power)	29.04	37.23	35.676	37.26	38.1029
Simulation (Frequency)	13.2	10.3	11	11	8.75
Experimental (Frequency)	13.28	10.09	11.1	10.86	8.66

Table 4-5: Simulation and experimental voltages, displacement, power and natural frequency of the system

References	Volume (cm^3)	Frequency (Hz)	Amplitude (m/s^2)	Power (W)	Power density (W/cm^3)
Glynne-Jones et al.[24]	0.84	322	2.7	1.80e-4	2.14e-4
Williams et al.[25]	0.0054	4,400	382	3.00e-7	5.56e-5
Ching et al.[12]	1	110	95.5	8.30e-4	8.30e-4
Beeby et al. [26]	0.15	52	0.589	4.60e-5	3.07e-4
Wang et al. [13]	3.15	280	10	1.72e-5	5.46e-6
Domme [27]	112	16	3.74	5.50e-3	4.91e-5
Saha et al. [28]	12.5	8	0.38	1.50e-3	1.20e-4
Hoffmann et al.[29]	0.68	390	88.29	5.00e-6	7.35e-6
Hadas et al. [30]	100.9	17	4.9	5.00e-3	4.96e-5

Table 4-6: Previously developed electromagnetic energy harvesters

Maximum power dissipation is 38 mW at acceleration level of 1g where the coil resistance is matched with load resistance of 37 Ω. Maximum achievable power density for this design is $5.84e-4\ w/cm^3$**.** Energy harvester developed in this thesis has power density which is much higher than the current available energy harvesters in the market and literature shown in

Table 4-6. Energy harvester developed can withstand harsh environments and is very easy to assemble and disassemble with very low maintenance required.

In summary, chapter 4 discussed the development of a non-linear energy harvesting system. Optimized magnet to iron pole ratio as well as magnet to coil ratios were used to develop an optimized energy harvesting system. Non-linear harvester is to be used for power equipment such as lawnmower and snow blower and any other vibrating equipment. By adding stationary top and bottom magnets on the optimized harvester, it was capable of operating as an inertial based harvester. Two tuning methods were used and it was shown that changing the air gap was more effective at changing the natural frequency. The designed harvester was prototyped such that it was easy to assemble so that it can be tuned depending on the vibrating natural frequency.

Chapter 5

Conclusion

In this thesis an electromagnetic energy harvesting system was developed based on Faraday's law. Chapter 1 gave a brief introduction of energy harvesting systems available for harvesting vibrational kinetic energy. Literature review was conducted on energy harvesting systems in chapter 2 that were developed by research institutes around the world. Kinetic based energy harvesters were looked at in detail and they were sectioned into three categories: Piezoelectric, electrostatic and electromagnetic. Flaws and benefits of each of the harvesters as well as their operating capabilities were described. Research motivation behind this project was to develop a low frequency electromagnetic energy harvesting system that is better in terms of power density. Potential applications for the energy harvesting system were described which included snow blower and lawnmower.

In Chapter 3, a linear energy harvesting system was developed. Electromagnetic working theory as well as the design was detailed. Linear energy harvester consisted of stator and mover. Stator comprises of coils, iron casing and coil holder while the mover has magnets, iron poles and holding rod. First prototype developed was based on the permanent magnet to iron ratio τ_m/τ_p of 1.25 and permanent magnet to coil ratio r_p/r_s of 0.73. Prototype was developed and tested to determine the maximum power output. Power output of the linear energy harvesting system was determined to be 38 mW at displacement of 7.2 mm and frequency of 35 Hz. Power density of the system was determined to be 4.44e-4 W/cm^3. Simulation was then done in comsol to optimize the linear energy harvesting system to make it more efficient. Coil ratio r_p/r_s was iterated from 0.575 to 0.8563 and for each coil ratio, the permanent magnet to iron pole ratio τ_m/τ_p was optimized. It was determined that the best magnet to iron pole ratio was 3.175 while the magnet to coil ratio of 0.7938 was chosen. The energy harvesting systems discussed so far were force based and did not have a working natural frequency so the applications for this type of energy harvester would be in

buoys for weather and wave detection applications, beacons and autonomous equipment on ports and finishing explorations.

In Chapter 4, optimized ratios were used to develop an energy harvesting system. The optimized energy harvesting system was tested to determine the power output of 284 mW and the power density was determined to be 2.738e-2 W/cm^3. Thereafter, two stationary magnets were added at the top and bottom to make the harvester inertial based and was called non-linear energy harvester. Vibration testing was done on snow blower and lawnmower to determine the vibrating natural frequency. The non-linear harvester was developed to be rugged and easy to assemble and disassemble for ease of maintenance and repair. Mechanical damping was characterized by inputting a step response into non-linear energy harvesting system to plot the decay in displacement of the mover. Least square approach was used to determine the mechanical damping. One of the main objectives of the non-linear harvester was that it should be easily tuneable to match the ambient frequency. Shift in natural frequency was studied by changing two parameters of the system, magnet thickness L_m (6.35 mm to 12.7 mm) and the gap L_g (70.74 mm to 83.45 mm)**.** It was determined that the change in gap L_g was more effective at tuning for the natural frequency of lawnmower rather than changing the magnet thickness. Non-linear harvester was tested at acceleration level of 1g while changing the frequency from 5-30 Hz. Maximum power output of the non-linear energy harvester was determined to be 38 mW when L_g = 83.45 mm and L_m = 9.525 mm with power density of $5.84e-4\ w/cm^3$**.** Newly developed energy harvester showed drastic improvements in power dissipation capabilities as compared to the harvesters in reported literatures. Both linear and non-linear energy harvesting system showed promising voltage and power capabilities and could very well be used to power wireless sensor networks.

5.1 Future Work

The linear and non-linear energy harvesting system showed promising results but there is still more room for improvements. Some of the improvements that can be made to the current energy harvesting system include but are not limited to:

1. Conduct simulation to determine the power capabilities of the system when the volume of the energy harvester changes so that the energy harvester can be scaled or miniaturized further to operate at its peak. Current energy harvesting system developed had volume constraint and the optimizations were done for the same volume size.

2. Develop a multi directional energy harvesting system. Kinetic vibrational energy is spread in multi directions. The current energy harvesting system is only capable of harvesting energy in either the x or y direction but not both at the same time. This reduces efficiency of the system as vibration in one of the direction is never used. Multi direction energy harvesting system should be capable of harvesting vibrations in all directions.

3. Develop low voltage AC to DC rectifier circuit and battery storage circuit to convert and store harnessed energy for future use. The voltage output of the system is low so the storage circuit and AC to DC circuit should be carefully designed such that the voltage and power drop within the circuit is low. Voltage also needs to be stepped up so a voltage doubler, tripler or quadrupler circuit should be looked at.

4. In this thesis, the maximum power dissipation capacity of a given energy harvesting device was achieved based matching the total coil resistance to the load resistance according to the maximum power transfer theorem. However, this is only true for a purely resistive system where the reactance is zero or negligible. For an energy harvesting system the coils consist of resistance, inductive and capacitive reactance. The inductive reactance of the coils can be determined from (5-1)**.** For a multi-layer coil such as the one presented previous in this thesis, the inductance can be determined based on Wheeler approximation[31] as:

$$L = \frac{31.6 \cdot r_c^{\,2} \cdot n^2}{6 \cdot r_c + 9 \cdot l + 10 \cdot (r_s - r_c)} \qquad (5\text{-}1)$$

Where the inductance L is in μH (microhenries), r_c is the inside radius of the coil in meters, r_s is the outside coil radius in meters, l is the thickness of the coil in meters and n is the number of turns in coil (refer to coil Figure 3-2). The dimensions and

values for the inside radius, outside radius as well as number of turns for the coil are shown in Table 4-1, while the thickness of the coil is 1.6 mm. Based on these parameters the inductance is determined to be 37.31 microhenries. System is considered purely resistive if inductance and capacitance is zero. For a purely resistive system the phase lag between the voltage and current is zero. The phase lag between the current and voltage in the energy harvesting system can be determined by electrical impedance. Electrical impedance is defined as measure of resistance to a current when voltage is applied. The electrical impedance is defined as:

$$Z = R + jX \tag{5-2}$$

Where R is the resistance and X is the reactance. The total reactance consists of capacitive reactance X_C and inductive reactance X_L:

$$X = X_L - X_C \tag{5-3}$$

The electrical impedance of the coil for the energy harvesting system in this thesis is determined as shown in (5-4) while the phase angle between the voltage and the current is determined as shown in (5-5).

$$Z = 2.13 + j0.00703 \tag{5-4}$$

$$\theta = \tan^{-1}\left(\frac{X}{R}\right) = 0.19^{\circ} \tag{5-5}$$

The phase angle for the energy harvesting system in this thesis is determined to be 0.19 degrees. The phase angle can be approximated as zero, as the phase angle between the voltage and current is extremely small. With this approximation, the energy harvesting system can be considered purely resistive and matching internal to external load can be used to find maximum power. However, for a system with inductance and capacitance, matching internal and external resistance is no longer valid. As a future work if we intend to induce inductance effect then impedance matching has to be done as explained in the following manner:

The inclusion or presence of inductance and capacitance leads to phase lead or lag between voltage and current; which requires impedance matching. The basis of impedance matching for the system now considers the mechanical and electrical

systems independently to maximize power output of the harvester. When these two quantities are equal to one another power will be achieved. Mechanical impedance is described as force acting on the system over the velocity of the system as shown in (5-6).

$$Z_{mech} = \frac{F}{v} \tag{5-6}$$

In a mechanical system, damper is a dashpot that resists motion for a given force input. The damping force is determined as (5-7)**.**

$$F_D = Dv \tag{5-7}$$

Where D is the mechanical damping coefficient of the system and v is the velocity. There are several methods of determine mechanical damping. One approach is based on the logarithmic decrement method that was presented in chapter 4.3**.** By substituting (5-7) into (5-6)**,** mechanical impedance of a damper can be determined as:

$$Z_D = D \tag{5-8}$$

A spring on the other hand is characterized by its spring stiffness which is defined as force over the displacement of spring from its natural equilibrium position and can be written as:

$$F_k = kx \tag{5-9}$$

Where k is the spring stiffness and x is the compression or extension of spring. For a given sinusoidal force, impedance of the spring can be determined:

$$Z_k = -j\frac{k}{\omega} \tag{5-10}$$

Where ω is angular frequency and k is the spring stiffness. When a force is applied to a system with only mass, the system tends to accelerate and can be characterized as:

$$F_m = ma \tag{5-11}$$

Where m is the mass and a is the acceleration of the mass. For a given sinusoidal force input, the impedance is determined to be:

$$Z_m = j\omega m \tag{5-12}$$

Where ω is the angular frequency and m is the mass. It should be noted that the impedance of mass is an imaginary quantity that depends on the angular frequency and

the magnitude of mass [32]. The total impedance when a mass spring and a damper is combined can be described as shown in (5-13)**.**

$$Z = j\omega m + D - j\frac{k}{\omega} \tag{5-13}$$

Impedance matching of systems within two domains (mechanical and electrical in this case) can be achieved through matching impedance directly (with a self-consistent unit system within the mechanical and electrical analogous) or by a quantity known as the quality factor (5-14). The quality factor represents the energy stored over the energy dissipated.

$$\mathrm{Q} = 2\pi\left(\frac{\text{Energy stored}}{\text{Energy dissipated per cycle}}\right) \tag{5-14}$$

Now if we consider a mechanical system consisting of a mass, spring, and damper the mechanical quality factor can be determined as shown in (5-15)**.**

$$Q_{Mech} = \frac{\sqrt{Mk}}{D} \tag{5-15}$$

Where M is the mass, k is the spring stiffness and D is the mechanical damping coefficient. Now if we consider the quality factor for an electrical system that consists solely of a resistor, the quality factor is equal to:

$$Q_R = 0 \tag{5-16}$$

The quality factor is zero for this electrical system because a resistor only dissipates energy and has no capacity to store energy. When this circuit configuration is present (solely resistance) the impedance matching formulation of the two domains based on quality factor is no longer valid due to (5-16**)** being zero. This is a case where the maximum power transfer theorem should be used to match the load resistance to coil resistance. For an electrical system consisting of an inductor, the quality factor is equal to:

$$Q_L = \frac{\omega_0 L}{R_L} \tag{5-17}$$

Where ω_0 is the resonance frequency of the inductor, L is the inductance and R_L is the resistance of the inductor. The quality factor of capacitor is equal to:

$$Q_C = \frac{1}{C\omega_0 R_C} \tag{5-18}$$

Where ω_0 is the resonance frequency of the capacitor, C is the capacitance, and R_C is the resistance of the capacitor. For a system that consists of a capacitor and an inductor, the individual quality factors (5-17) and (5-18**)** yields:

$$Q = \frac{1}{\left(\frac{1}{1/Q_L + 1/Q_C}\right)} \tag{5-19}$$

If a resistor was added to a circuit with a capacitor and an inductor it would form a RLC circuit. The quality factor for a series RLC circuit is equal to:

$$Q_{Elec} = \frac{1}{R}\sqrt{\frac{L}{C}} = \frac{\omega_0 L}{R} \tag{5-20}$$

Where ω_0 is the resonance frequency, L is the inductance, C is the capacitance and R is the resistance of the entire circuit. Now by equating the mechanical and electrical quality factors the maximum power output of the harvester can be achieved based on (5-21)**.**

$$Q_{Elec} = Q_{Mech} \tag{5-21}$$

References

[1] A. S. Jonnalagadda, “Magnetic Induction Systems to Harvest Energy from Mechanical Vibrations,” 2007.

[2] P. Glynne-Jones, S. P. Beeby, and N. M. White, “Towards a piezoelectric vibration-powered microgenerator,” *IEE Proc. - Sci. Meas. Technol.*, vol. 148, no. 2, p. 68, 2001.

[3] S. L. Kok, N. M. White, and N. R. Harris, “Free-standing thick-film piezoelectric multimorph cantilevers for energy harvesting,” *2009 IEEE Int. Ultrason. Symp.*, pp. 1977–1980, Sep. 2009.

[4] N. S. Shenck and J. A. Paradiso, “ENERGY SCAVENGING WITH SHOE-MOUNTED PIEZOELECTRICS,” *IEEE*, vol. 21, no. 3, pp. 30–42, 2001.

[5] H.-B. Fang, J.-Q. Liu, Z.-Y. Xu, L. Dong, L. Wang, D. Chen, B.-C. Cai, and Y. Liu, “Fabrication and performance of MEMS-based piezoelectric power generator for vibration energy harvesting,” *Microelectronics J.*, vol. 37, no. 11, pp. 1280–1284, Nov. 2006.

[6] B. Ziaie, “Low frequency wireless powering of microsystems,” pp. 1707–1710, 2003.

[7] Y. B. Jeon, R. Sood, J. -h. Jeong, and S.-G. Kim, “MEMS power generator with transverse mode thin film PZT,” *Sensors Actuators A Phys.*, vol. 122, no. 1, pp. 16–22, Jul. 2005.

[8] S. Meninger, J. O. Mur-Miranda, R. Amirtharajah, a. Chandrakasan, and J. H. Lang, “Vibration-to-electric energy conversion,” *IEEE Trans. Very Large Scale Integr. Syst.*, vol. 9, no. 1, pp. 64–76, Feb. 2001.

[9] R. Tashiro, N. Kabei, K. Katayama, E. Tsuboi, and K. Tsuchiya, “Development of an electrostatic generator for a cardiac pacemaker that harnesses the ventricular wall motion,” *J. Artif. Organs*, vol. 5, no. 4, pp. 239–245, Dec. 2002.

[10] Y. Naruse, N. Matsubara, K. Mabuchi, M. Izumi, and S. Suzuki, “Electrostatic micro power generation from low-frequency vibration such as human motion,” *J. Micromechanics Microengineering*, vol. 19, no. 9, p. 094002, Sep. 2009.

[11] R. Torah, P. Glynne-Jones, M. Tudor, T. O’Donnell, S. Roy, and S. Beeby, “Self-powered autonomous wireless sensor node using vibration energy harvesting,” *Meas. Sci. Technol.*, vol. 19, no. 12, p. 125202, Dec. 2008.

[12] N. N. H. Ching, H. Y. Wong, W. J. Li, P. H. W. Leong, and Z. Wen, “A laser-micromachined multi-modal resonating power transducer for wireless sensing systems,” *Sensors Actuators A Phys.*, vol. 97–98, pp. 685–690, Apr. 2002.

[13] P. Wang, X. Dai, X. Zhao, and G. Ding, “A MICRO ELECTROMAGNETIC VIBRATION ENERGY HARVESTER WITH SANDWICHED STRUCTURE AND AIR CHANNEL FOR HIGH ENERGY CONVERSION EFFICIENCY,” pp. 4–7, 2009.

[14] P. Glynne-Jones, M. J. Tudor, S. P. Beeby, and N. M. White, “An electromagnetic, vibration-powered generator for intelligent sensor systems,” *Sensors Actuators A Phys.*, vol. 110, no. 1–3, pp. 344–349, Feb. 2004.

[15] B. J. Bowers and D. P. Arnold, “Spherical, rolling magnet generators for passive energy harvesting from human motion,” *J. Micromechanics Microengineering*, vol. 19, no. 9, p. 94008, Sep. 2009.

[16] N. Fondevilla, C. Serre, a Perez-Rodriguez, M. C. Acero, E. Cabruja, H. Campanella, and J. Esteve, “Electromagnetic harvester device for scavenging ambient mechanical energy with slow, variable, and randomness nature,” *2011 Int. Conf. Power Eng. Energy Electr. Drives*, no. May, pp. 1–5, 2011.

[17] B. Yang, C. Lee, W. Xiang, J. Xie, J. Han He, R. K. Kotlanka, S. P. Low, and H. Feng, “Electromagnetic energy harvesting from vibrations of multiple frequencies,” *J. Micromechanics Microengineering*, vol. 19, no. 3, p. 035001, 2009.

[18] A. R. M. Foisal and G.-S. Chung, “Design and Analysis of a Vibration-driven AA Size Electromagnetic Energy Harvester Using Magnetic Spring,” *Trans. Electr. Electron. Mater.*, vol. 13, no. 3, pp. 125–128, Jun. 2012.

[19] V. R. Challa, M. G. Prasad, and F. T. Fisher, “A coupled piezoelectric–electromagnetic energy harvesting technique for achieving increased power output through damping matching,” *Smart Mater. Struct.*, vol. 18, no. 9, p. 095029, Sep. 2009.

[20] P. Patel and M. B. Khamesee, “Electromagnetic micro energy harvester for human locomotion,” *Microsyst. Technol.*, Jun. 2013.

[21] “Permanent Magnet Selection and Design Handbook.”

[22] B. Ebrahimi, “Development of Hybrid Electromagnetic Dampers for Vehicle Suspension Systems,” 2009.

[23] P. Patel and M. B. Khamesee, “Microenegy harvesting applications for outdoor power equipment,” *ASME-ISPS Proceeding*, 2013, 3 pp.

[24] S. Beeby, M. Tudor, and N. White, “Energy harvesting vibration sources for microsystems applications,” *Meas. Sci. Technol.*, vol. 17, no. 12, pp. R175–R195, Dec. 2006.

[25] C. B. Williams, C. Shearwood, M. a. Harradine, P. H. Mellor, T. S. Birch, and R. B. Yates, “Development of an electromagnetic micro-generator,” *IEE Proc. - Circuits, Devices Syst.*, vol. 148, no. 6, p. 337, 2001.

[26] S. P. Beeby, R. N. Torah, M. J. Tudor, P. Glynne-Jones, T. O’Donnell, C. R. Saha, and S. Roy, “A micro electromagnetic generator for vibration energy harvesting,” *J. Micromechanics Microengineering*, vol. 17, no. 7, pp. 1257–1265, Jul. 2007.

[27] D. J. Domme, A. J. Kurdila, and M. Johnson, “Experimental and Analytical Characterization of a Transducer for Energy Harvesting Through Electromagnetic Induction,” 2008.

[28] C. R. Saha, T. O’Donnell, N. Wang, and P. McCloskey, “Electromagnetic generator for harvesting energy from human motion,” *Sensors Actuators A Phys.*, vol. 147, no. 1, pp. 248–253, Sep. 2008.

[29] D. Hoffmann, B. Folkmer, and Y. Manoli, “Fabrication, characterization and modelling of electrostatic micro-generators,” *J. Micromechanics Microengineering*, vol. 19, no. 9, p. 094001, Sep. 2009.

[30] Z. Hadas, C. Ondrusek, and V. Singule, “Power sensitivity of vibration energy harvester,” *Microsyst. Technol.*, vol. 16, no. 5, pp. 691–702, Feb. 2010.

[31] Wheeler, H.A., "Simple Inductance Formulas for Radio Coils," Radio Engineers, Proceedings of the Institute of , vol.16, no.10, pp.1398,1400, Oct. 1928

[32] Hixson, E.L.:"Mechanical Impedance and Mobility," Chap.10, in C.M. Harris and E.E.Crede (eds.),"Shock and Vibration Handbook," 1st ed.,McGraw-Hill Book Company, New York, 1961.